Article

Climate change and terrigenous inputs decrease the efficiency of the future Arctic Ocean's biological carbon pump

Laurent Oziel [1] ✉, Özgür Gürses[1], Sinhué Torres-Valdés [1], Clara J. M. Hoppe [1], Björn Rost [1,2], Onur Karakuş[1,3], Christopher Danek [1], Boris P. Koch [1,4], Cara Nissen [1,5], Nikolay Koldunov [1], Qiang Wang [1], Christoph Völker [1], Morten Iversen [1,6], Bennet Juhls[7] & Judith Hauck [1]

The Arctic experiences climate changes that are among the fastest in the world and affect all Earth system components. Despite expected increase in terrigenous inputs to the Arctic Ocean, their impacts on biogeochemical cycles are currently largely neglected in IPCC-like models. Here we used a state-of-the-art high-resolution ocean biogeochemistry model that includes carbon and nutrient inputs from rivers and coastal erosion to produce twenty-first-century pan-Arctic projections. Surprisingly, even with an anticipated rise in primary production across a wide range of emission scenarios, our findings indicate that climate change will lead to a counterintuitive 40% reduction in the efficiency of the Arctic's biological carbon pump by 2100, to which terrigenous inputs contribute 10%. Terrigenous inputs will also drive intense coastal CO_2 outgassing, reducing the Arctic Ocean's carbon sink by at least 10% (33 TgC yr^{-1}). These unexpected reinforced feedback, mostly due to accelerated remineralization rates, lower the Arctic Ocean's capacity for sequestering carbon.

In the Arctic, anthropogenic climate change is causing one of the most rapid and profound climate transformations on the planet[1]. Remote-sensing studies estimate that net primary production (NPP) in the Arctic Ocean (AO) has linearly increased by 56% during the past two decades due to enhanced light (caused by increased ice melt) and nutrient availability[2]. As a result of the 'AO Amplification' (that is, the warming of the AO at twice the global average rate[3]), it is expected that the AO will experience ice-free summers by 2050[4]. IPCC-like models (Earth system models, used by the United Nation's IPCC, also referred to as Coupled Model Intercomparison Project Phase 6) recently came to a consensus where NPP is still expected to increase in the future[5]. However, more nutrients are needed to support the increasing NPP in surface waters. Nitrogen is considered to be the main limiting nutrient in the AO[6] and its availability is becoming the 'bottleneck' of the AO's productivity. At the same time, climate change is intensifying permafrost thaw[7–9], coastal erosion[10,11] and river run-off[12,13], potentially resulting in tremendous quantities of carbon and nutrients being delivered to the AO. Most models neglect these terrigenous inputs, coastal erosion in particular, even though a recent study suggests that the associated nutrient supply may fuel more than 30% of the contemporary NPP in the AO[14].

In this study, we investigate the biological carbon pump[15] (BCP). The BCP is the suite of processes that mediate transport of carbon of biological origin from the surface ocean to depth, impacting the AO's carbon sink by lowering the partial pressure of CO_2 in the surface ocean

[1]Alfred-Wegener-Institut - Helmholtz-Zentrum für Polar- und Meeresforschung, Bremerhaven, Germany. [2]Faculty of Biology/Chemistry, University of Bremen, Bremen, Germany. [3]Physical Oceanography Department, Woods Hole Oceanographic Institution, Woods Hole, MA, USA. [4]Faculty 1, Bremerhaven University of Applied Sciences, Bremerhaven, Germany. [5]Department of Atmospheric and Oceanic Sciences and Institute of Arctic and Alpine Research, University of Colorado Boulder, Boulder, CO, USA. [6]MARUM and University of Bremen, Bremen, Germany. [7]Alfred Wegener Institute, Helmholtz Centre for Polar and Marine Research, Potsdam, Germany. ✉e-mail: laurent.oziel@awi.de
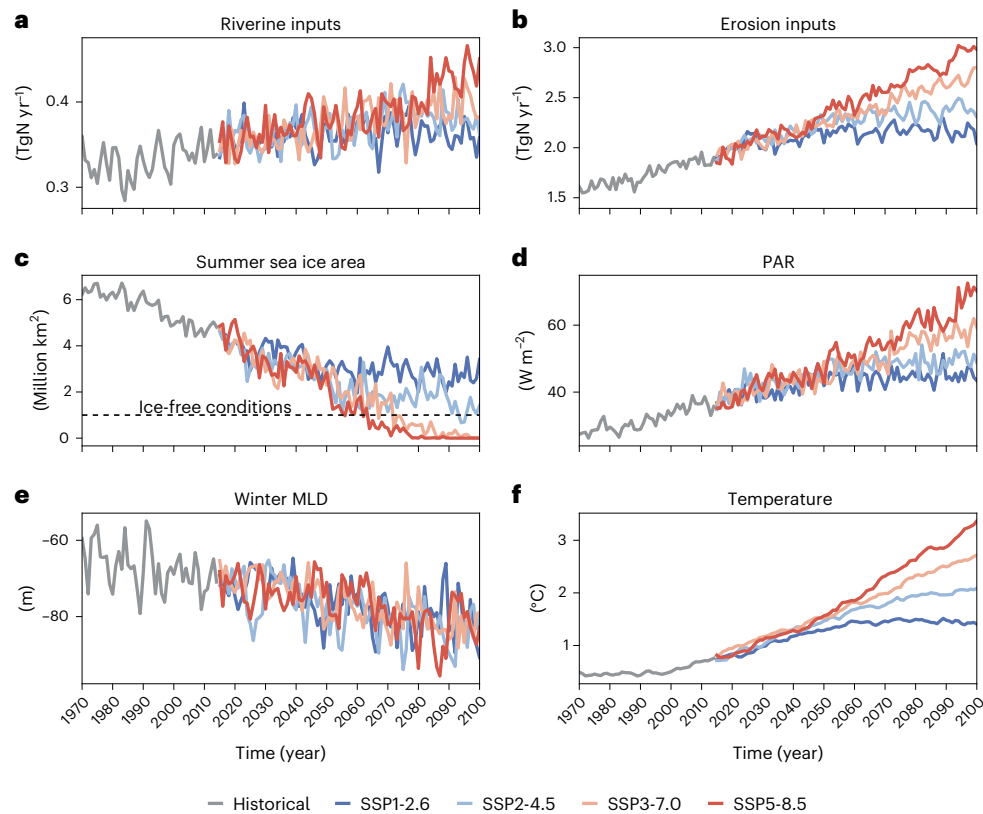
Fig. 1 | Characteristics of the 'New' Arctic Ocean. a,b, Time series of nitrogen inputs from rivers (**a**) and coastal erosion (**b**). **c–f**, Time series of environmental conditions over the AO during the historical (1970–2014) and forecast (2015–2100) periods with summer (September) sea ice area (million km²) (**c**), annual photosynthetically active radiation at the ocean surface (W m⁻²) (**d**), winter (March) mixed layer depth (MLD) (m) (**e**) and averaged temperature in the upper mesopelagic layer (100–600 m) (°C) (**f**).

(p_{CO_2})[16,17]. More specifically, we focus on the export of particulate organic carbon, that is, the gain side of the 'soft-tissue' pump, although we acknowledge that losses occur through ventilation[18]. We assume the 'soft-tissue' pump to be responsible for most of the vertical gradient of carbon in the AO mainly because the 'hard-tissue' pump (or carbonate pump) is much weaker (Supplementary Fig. 1) and increases surface p_{CO_2} during calcification. Furthermore, physical vertical transport is hindered by the presence of a permanent halocline (a density barrier below the mixed layer[19]), strong stratification[20] and low vertical mixing[21]. As the first step of the BCP, primary producers, largely dominated by phytoplankton, perform photosynthesis. Photosynthesis produces organic matter by assimilating nutrients and carbon (that is, NPP), thereby removing CO_2 from surface waters and favouring atmospheric CO_2 uptake. Phytoplankton can form aggregates or are grazed by zooplankton, which assimilate them or pack them into faecal pellets. Both phytoplankton aggregates and zooplankton faecal pellets are considered particulate organic detritus, which sinks out of the upper sunlit layers, driving the export and sequestration flux of carbon and nutrients (the export of organic detritus through the 100 m and 600 m horizons, respectively; Methods) into the mesopelagic ocean[22]. Remineralization is a pivotal process that degrades the organic matter back to its inorganic form. As a metabolic respiratory mechanism, remineralization is primarily governed by temperature[23] and consequently exhibits a high sensitivity to warming[24,25]. It also controls the efficiency of the BCP[26,27] by (1) attenuating the export flux of carbon, (2) replenishing the ocean with 'new' nutrients and (3) modulating CO_2 concentration in the surface ocean and thereby, exchanges with the atmosphere[28].

To quantify the future impacts of climate change-induced warming and increasing terrigenous inputs of carbon and nutrients on the efficiency of the BCP in the AO, we provide four metrics[18,29,30] (Methods):

(1) the change in seawater p_{CO_2} due to biological activity, (2) the export efficiency, that is, the AO's capacity to export the organic matter produced at the surface to deeper water layers (export flux/NPP), (3) the transfer efficiency, that is, the capacity of the AO to sequester organic matter for centuries to millennia (sequestration flux/export flux) and (4) the storage of carbon of biological origin in the ocean interior (DIC_{REMIN}). The BCP efficiency therefore encapsulates the AO's capacities to fix carbon and to produce, export, sequester and store organic matter for centuries to millennia. To reach our objectives, we derived a suite of transient (varying climate and CO_2 forcing) hindcast and forecast simulations as well as a control simulation with constant climate (1970–2100; Extended Data Table 1). We used the global 'state-of-the-art' ocean and sea ice biogeochemistry model FESOM2.1-REcoM3 (ref. 31). We specifically configured and tuned the model for the AO, with an eddy-permitting horizontal resolution of 4.5 km at the pan-Arctic scale. We derived a simulation with a high-emission future scenario (Shared Socioeconomic Pathway SSP3-7.0 (ref. 32)), including varying inputs of carbon and nutrients from rivers and coastal erosion (Fig. 1a,b) as our baseline simulation, also referred to as 'Terr'. We conducted a reference simulation with the same configuration as Terr but without any terrigenous inputs (referred to as 'NoTerr'). We also repeated Terr but with different emission scenarios (from low to high: SSP1-2.6, SSP2-4.5 and SSP5-8.5).

With those simulations, after characterizing the emerging properties of the 'new Arctic', we separately quantify the impacts of climate change (including CO_2 feedback) and terrigenous inputs on carbon and nitrogen budgets (Fig. 2 and Extended Data Table 2). We define climate change as the difference between the 2090s and the 1970s in the Terr simulation (SSP3-7.0). The role of terrigenous inputs is defined as the difference between Terr and noTerr in the 2090s (SSP3-7.0).
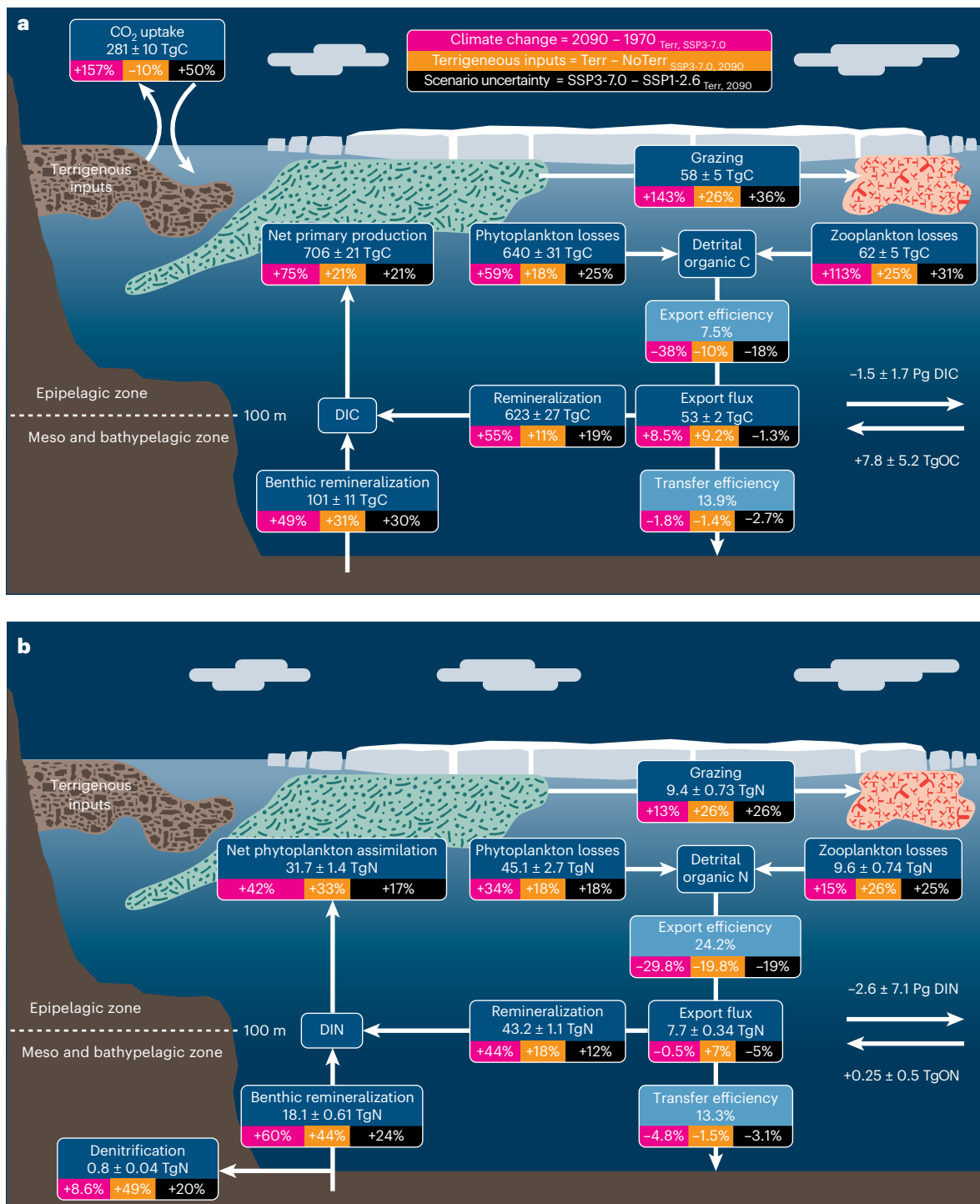
Fig. 2 | Simplified carbon and nitrogen budgets for the AO. a,b, Budgets for carbon (**a**) and nitrogen (**b**). Absolute quantities are expressed in carbon (TgC yr⁻¹) and nitrogen (TgN yr⁻¹) and refer to the baseline simulation Terr (with terrigenous inputs) by the end of the century (2090s). Relative contributions (%) of climate change (2090s relative to 1970s, with Terr, SSP3-7.0 emission scenario) and terrigenous inputs (Terr relative to NoTerr in the 2090s) are shown in pink and orange, respectively. The scenario uncertainty (SSP3-7.0 relative to SSP1-2.6 in the 2090s) is indicated in black. Phytoplankton losses encompass excretion and aggregation. Zooplankton losses encompass mortality, excretion, sloppy feeding and faecal loss. Horizontal arrows on the right represent transport with the adjacent seas. DIC, dissolved inorganic carbon; OC, organic carbon; DIN, dissolved inorganic nitrogen; ON, organic nitrogen. Detrital organic matter encompasses both dissolved and particulate non-planktonic (detritus) pools.

In addition, we investigate the 'scenario uncertainty', corresponding to a shift from a high to a low-emission scenario (SSP3-7.0 minus SSP1-2.6, both with terrigenous inputs, in the 2090s). Finally, we discuss the implications for the Arctic ecosystem and biogeochemical cycles. We demonstrate that climate change and terrigenous inputs are responsible for unexpected positive feedback in the AO's biogeochemical cycles, dampening the efficiency of the BCP and impoverishing the AO's ecosystem.

Towards the 'new Arctic'

In the context of climate change, the AO inexorably shifts towards a new state (Fig. 1), often referred to as the 'new Arctic'[33]. As expected,
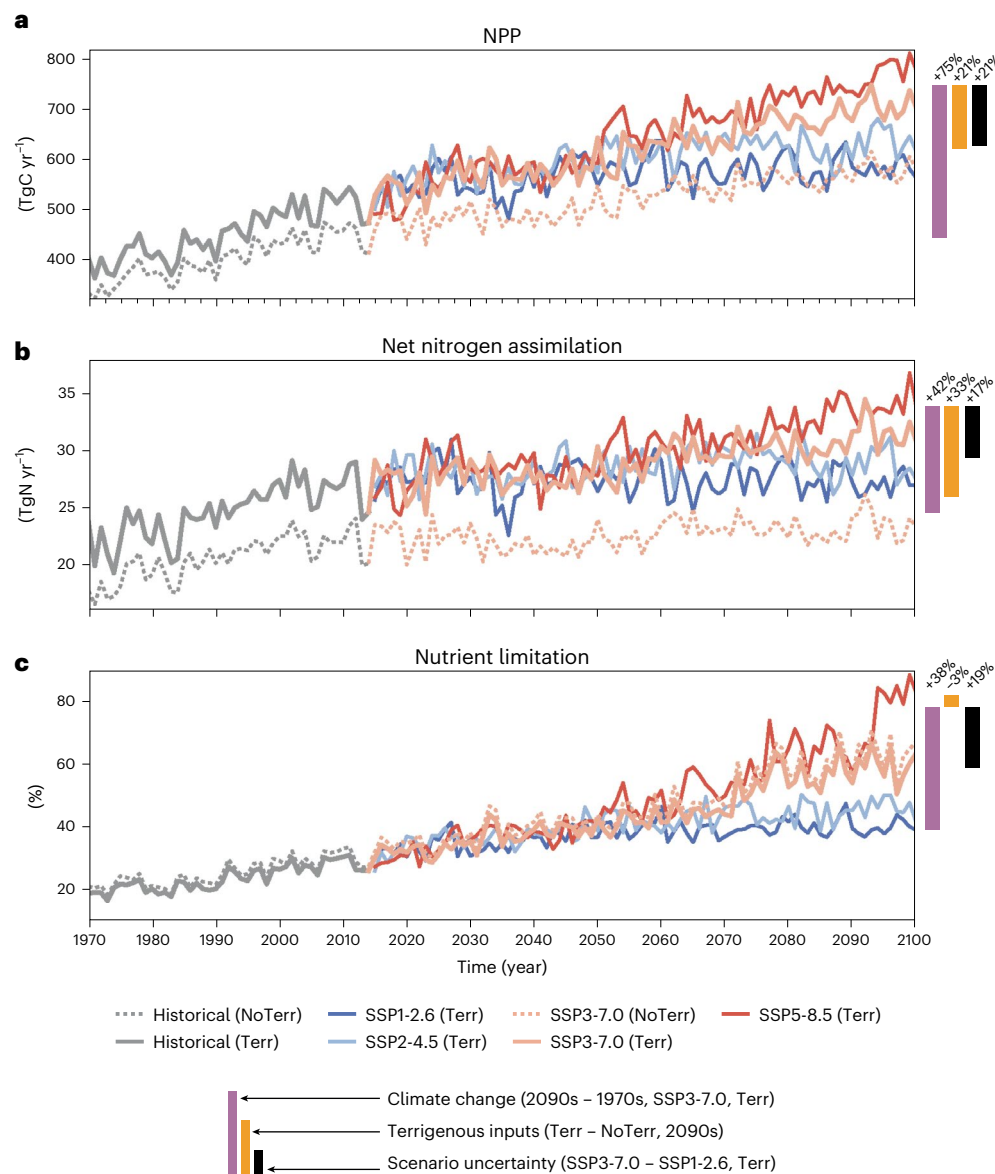
Fig. 3 | Primary productivity and nutrient drawdown. a–c, Time series over the AO during the historical (1970–2014) and forecast (2015–2100) periods of integrated net primary production (TgC yr^{-1}) (**a**), integrated net nitrogen assimilation rate (TgN yr^{-1}) (**b**) and averaged (over the surface layer, 0–50 m) summer (September) percentage of the AO area limited by nutrients (%) (**c**). Bars on the right represent the contributions of climate change (purple), terrigenous inputs (orange) and the scenario uncertainty (black).

our simulations show that the 'new Arctic' (studied area roughly north of 66.5° N; Extended Data Fig. 1) experiences future sea ice loss. Ice-free summers are frequent in the second half of the century under the two high-emission scenarios (Fig. 1c), as also observed in other studies[34]. The loss and thinning of sea ice allows for increased light availability[35]. In our model, surface photosynthetically active radiation (PAR) is inversely correlated with the sea ice area, doubling from ~30 to ~60 W m^{-2} with climate change (Fig. 1d). The climate change response with regards to winter mixing and stratification (Methods) is more subtle, probably due to regional compensating effects of freshwater and sea ice decline[36]. In winter, our model projects a general deepening of the mixed layer depth by 15 m (Fig. 1e) and a weakening stratification by -0.15 kg m^{-3} (Extended Data Fig. 2a) by 2100, in line with IPCC-like models[37].

In our Terr simulation, we mostly attribute the 75% NPP increase by the end of the century (Figs. 2a and 3a) to warming, subsequent sea ice decline and increase in light availability. Such NPP stimulation increases net nitrogen assimilation by phytoplankton by 42% (Figs. 2b and 3b), which will progressively shift the AO from a light-limited

system to a nutrient-limited system (from ~20% of the AO area limited by nutrients in the 1970s to ~60–80% in the 2090s; Fig. 3c). This climate-driven shift towards a more nutrient-limited AO, in line with previous expectations[6,15], is reflected in the phytoplankton community and elemental stoichiometry. Our results confirm a compositional shift towards a dominance of small phytoplankton over diatoms[38,39] (Supplementary Fig. 2), with increasing phytoplankton C:N ratios (Supplementary Fig. 3). Eventually, phytoplankton elemental stoichiometry is transferred to detritus properties (Extended Data Fig. 2c). One could therefore expect a classic negative feedback loop on atmospheric CO_2 (Fig. 4a and Methods), where less sea ice drives more light availability, more NPP and more carbon export flux, and ultimately favours the uptake of atmospheric CO_2 by the AO.

Unexpected positive feedback in the biogeochemical cycles

A negative feedback loop could potentially even be enhanced by increasing terrigenous inputs (stimulating NPP) and higher C:N ratios
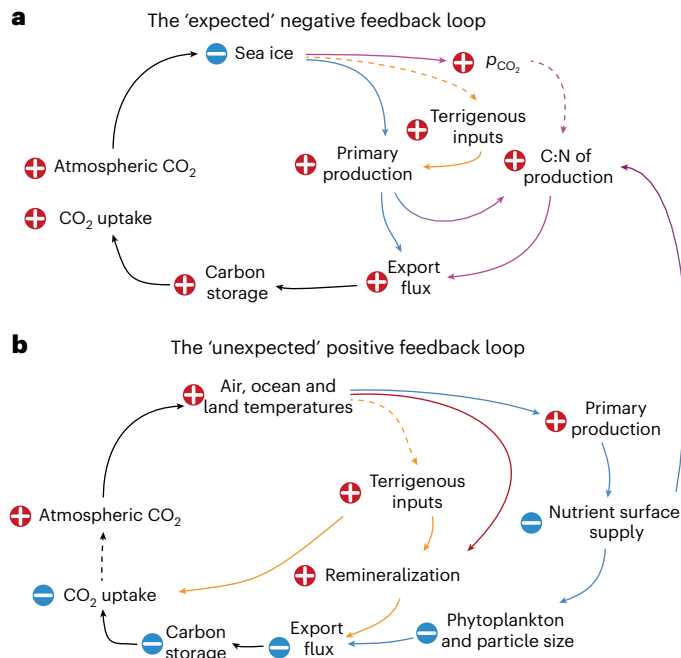
a The 'expected' negative feedback loop

b The 'unexpected' positive feedback loop

Fig. 4 | Feedback loops in the BCP driven by climate change and terrigenous inputs. a,b, Mechanisms are separated into those that are likely to have negative (**a**) or positive (**b**) feedback. Note that the arrow from export flux to CO_2 fluxes encompasses changes in surface DIC concentration and p_{CO_2}. Dashed arrows are processes, which are not demonstrated in this study.

(favouring export flux of carbon against nitrogen) in the future. However, we found that another, in fact positive feedback loop increases its prevalence with respect to the BCP (Fig. 4b).

Climate- and CO_2-driven feedback

The observed strong increase in CO_2 uptake by the AO (Fig. 5a) is driven by climate change (2090s – 1970s, Terr, SSP3-7.0). Temporal changes in our results cannot be attributed to the small model drift (Extended Data Fig. 3), which shows that the surface and intermediate oceans reach a quasi-equilibrium. However, most of the increase is driven by abiotic processes such as sea ice loss[40] and increasing atmospheric CO_2 concentration (Supplementary Figs. 4 and 5). This results in an increase in seawater p_{CO_2} (Fig. 5b), which in turn increases the Revelle factor (Methods and Fig. 5c). A greater Revelle factor translates into a decrease in the 'buffer' capacity of the AO[41], that is, a chemically less-efficient atmospheric CO_2 uptake by the ocean. However, a higher Revelle factor also amplifies the effect of seasonal drivers on the CO_2 uptake[30] and may thus alter the biologically driven CO_2 drawdown. In the AO, the CO_2 drawdown by biological activity in the surface layer is small and declines to a state of CO_2 enrichment in some years of the end of the twenty-first century (Fig. 5d). Therefore, counterintuitively, more NPP does not necessarily translate into greater biological CO_2 drawdown due to the increased prevalence of respiratory processes, which also exceed the effect of the Revelle factor (Supplementary Fig. 6).

A first explanation lies in the functioning of the ecosystem. In line with the usual paradigm that changes in the lower trophic level cascade up the food chain[42], we find that more NPP is generally accompanied by increased zooplankton grazing both in terms of carbon and nitrogen (Fig. 2). We found that this leads to greater losses of organic detritus from plankton to the surrounding seawater. Together with warming, the amplifying size of the organic matter reservoir instigates substantial enhancement of remineralization rates. Indeed, remineralization is not only sensitive to temperature, but also to the size (and quality) of the organic matter reservoir[43–45]. Here we quantify that carbon and

nitrogen remineralization increase by 55% and 44%, respectively, due to climate-driven feedback (Figs. 2 and 6a). This increase in remineralization is the fastest in the central AO, in particular in the Eurasian basin (Supplementary Fig. 7). While most of the increase in remineralization occurs at the surface, it also increases beneath the surface layer (Supplementary Fig. 8). Plankton respiration and remineralization (mainly driven by bacteria[46]) dominate over photosynthetic processes at depth (Supplementary Fig. 9) and are particularly sensitive to temperature changes[23]. We project a mesopelagic end-of-century warming of the AO (Fig. 1f; SSP3-7.0) that surpasses that of the global ocean by ~1.8 times. Enhanced mesopelagic respiration rates (that is, remineralization), together with a decrease in solubility due to warming, decrease the mesopelagic oxygen concentrations (Extended Data Fig. 2b).

Increased remineralization has negative impacts on export fluxes, sequestration and the storage of carbon of biological origin in the ocean interior. Both carbon and nitrogen export fluxes experienced a change point in the linear trend occurring in the 2010s (Methods, Fig. 6c,e and Supplementary Fig. 10). This suggests that most of their increase occurred before this period, while they are expected to stagnate or even decrease in the future compared with present levels. This can be explained by the fact that remineralization increases faster than the ability of the AO to export organic detritus. Consequently, the remineralization efficiency (defined as the ratio between the remineralization rate and the export flux) increases by up to 40% (Fig. 6b). This fuels the positive feedback loop (Fig. 4b) and reduces the export efficiency (C: −38%, N: −30%; Fig. 6d,f). These findings are corroborated by the analysis of the Coupled Model Intercomparison Project Phase 6 (CMIP6) ensemble (Extended Data Figs. 4 and 5). In our model, only a small share of the exported organic detritus is sequestered below 600 m, as illustrated by the transfer efficiencies (C: 13.9%, N: 13.3%; Fig. 2), and those numbers are decreasing further with climate change (C: −1.8%, N: −4.8%). Increasing remineralization also translates to a less-efficient carbon storage. Indeed, the strength of the BCP should also be measured by DIC_{REMIN}, a metric for the reservoir of carbon of biological origin in the ocean interior[18]. With climate change, DIC_{REMIN} decreases by 13%, confirming a weakening BCP (Fig. 6e). This reduced accumulation of DIC_{REMIN} within the AO's interior, in the context of a stagnating export flux, must be attributed to other 'losses' through physical transport, either laterally towards the global ocean (Extended Data Fig. 6) or vertically to the surface layer. The re-emergence of dissolved inorganic carbon (DIC) at the surface would further dampen the chemical buffering (that is, increase Revelle factor) or promote outgassing, creating another chemical positive feedback loop.

Terrigenous input-driven feedback

Terrigenous inputs can affect the AO's BCP through the release of dissolved inorganic or organic carbon, alkalinity and nutrients. In fact, terrigenous inputs (Terr − NoTerr, 2090s, SSP3-7.0) slightly increase the partial pressure of CO_2 in the surface ocean (Fig. 5b). This is due to the combination of carbon release, negligible effect on chemical uptake capacities at pan-Arctic scale (Fig. 5c and Supplementary Fig. 5k) and a strong decrease in p_{CO_2} drawdown due to biological activity by up to 16% (Fig. 5d). Consequently, our results indicate that terrigenous inputs are actually responsible for intense CO_2 outgassing at the pan-Arctic scale, with ~32.7 ± 3.3 TgC yr^{-1} for the 2090s (Extended Data Fig. 7), more than 50% of Spain's CO_2 emissions in 2021[47] (equivalent to 120 GtCO$_2$ yr^{-1}). Most of the outgassing occurs on continental shelves, supporting recent regional findings[48,49]. Terrigenous inputs therefore reduce the AO's carbon sink by releasing large quantities of CO_2 to the atmosphere.

Terrigenous inputs stimulate NPP (+21.4%), net nitrogen assimilation (+33%; Figs. 2 and 3) but also remineralization (C: +11%, N: +18%; Figs. 2 and 6). Similar to the climate-driven response discussed above, terrigenous inputs cause escalating losses of detritus emanating from both phytoplankton and zooplankton (Fig. 2), expanding the size of
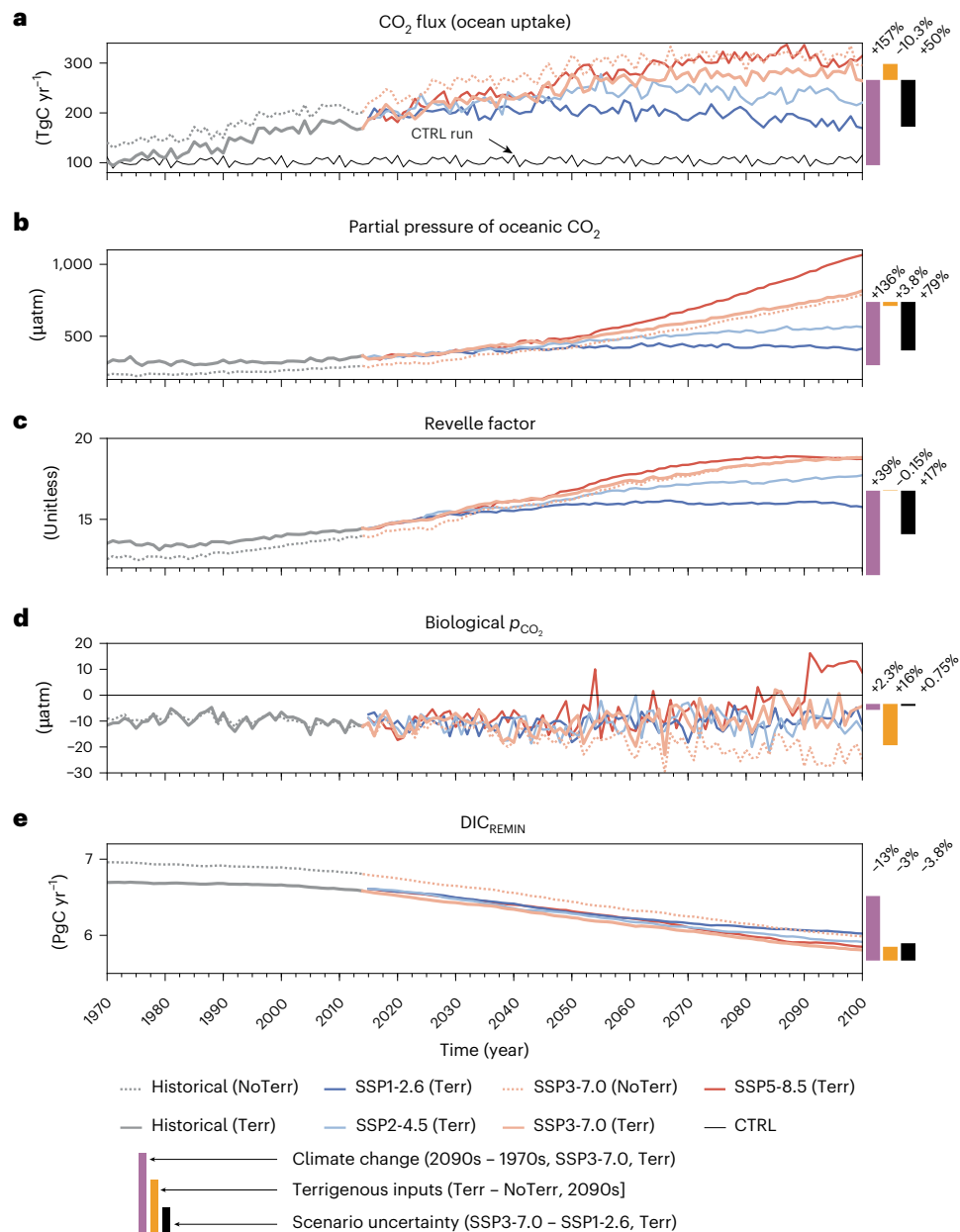
Fig. 5 | Carbon sink, budget and storage. a–e, Time series of metrics illustrating the evolution of the carbon budgets over the AO during the historical (1970–2014) and forecast (2015–2100) periods: carbon sink (air–sea CO_2 flux, positive being uptake) (TgC yr^{-1}) (**a**); partial pressure of CO_2 in the surface ocean (μatm) (**b**); the Revelle factor (unitless) (**c**), illustrating the chemical uptake or 'buffer' capacity; the biologically driven change in surface ocean p_{CO_2} (negative being CO_2 drawdown) (μatm) (**d**); and DIC$_{REMIN}$ illustrating the storage of carbon of biological origin (PgC yr^{-1}) (**e**). Bars on the right represent the contributions of climate change (purple), terrigenous inputs (orange) and scenario uncertainty (black).

the organic pool. Consequently, water-column remineralization provides the largest nitrogen inventory increase among biogeochemical processes with +6.5 TgN (Extended Data Table 2). Terrigenous inputs also induce +44% and +31% increases in benthic nitrogen and carbon remineralization, respectively (Fig. 2), which, combined with pelagic remineralization, represent the major biogeochemical source of inorganic matter.

Surprisingly, terrigenous inputs seem to increase remineralization faster than organic matter production and export, also fuelling the positive feedback loop (Fig. 4b). The increase in export fluxes remains limited (C: 9%, N: 7%; Figs. 2 and 6) compared with NPP (+21.4%) and remineralization (+18%). This may be explained by the fact that remineralization is influenced by the size of the organic pool and temperature, whereas NPP is also limited by inorganic nutrients. As a result, the

remineralization efficiency increases by about +10% with terrigenous inputs, resulting in a decrease in the export efficiency (C: −10%, N: −19.8%; Fig. 6d,f). This terrigenous-stimulated change is substantial, as it has the same order of magnitude as the changes induced by about one century of climate change. Through the same mechanisms, terrigenous inputs decrease the transfer efficiency and DIC$_{REMIN}$ by about −1.5% (Fig. 2) and −3% (Fig. 5e), respectively, corroborating the decline in the BCP efficiency.

Scenario uncertainty
Scenario uncertainty (SSP3-7.0 − SSP1-2.6, Terr, 2090s) represents a 50% spread in the AO's carbon sink projections for the same abiotic reasons (sea ice and atmospheric CO_2 concentration) as climate- and CO_2-driven feedback change (Supplementary Fig. 5). Across all emission
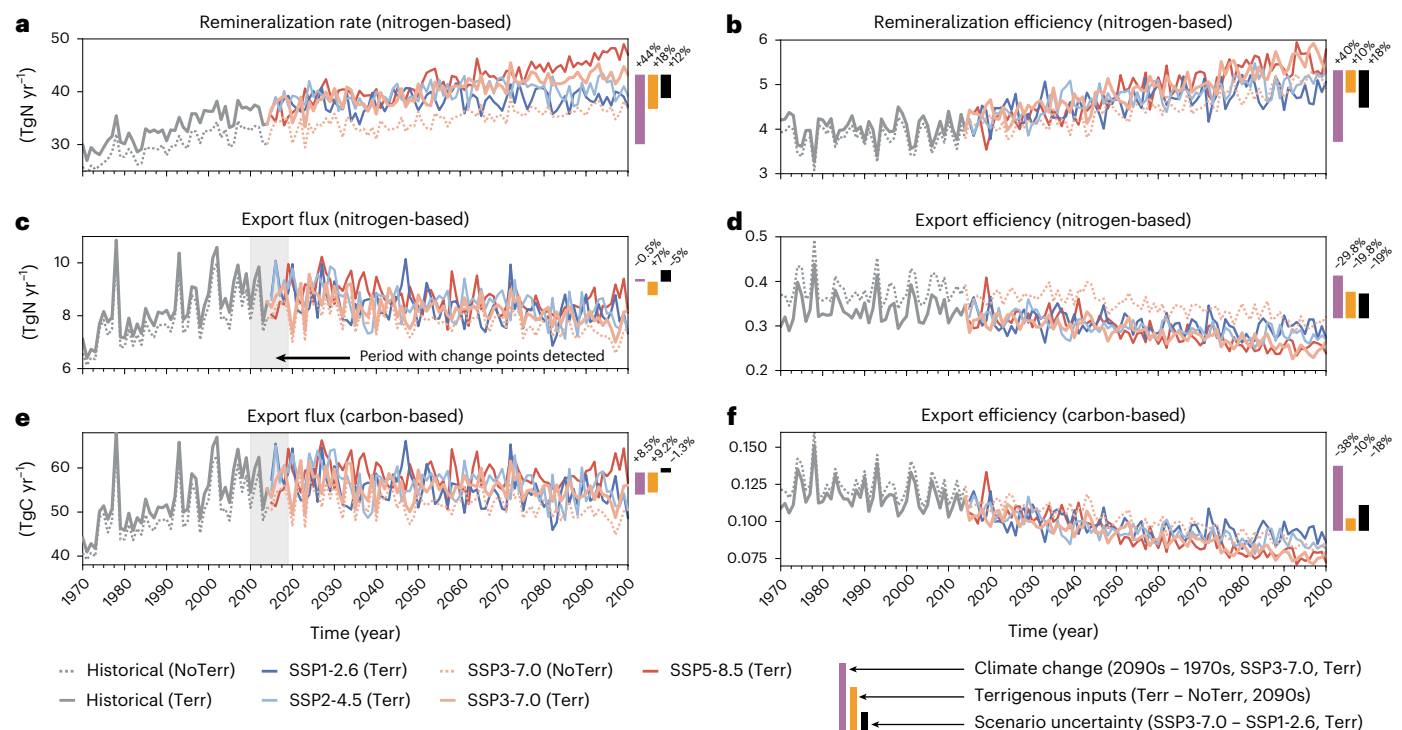
Fig. 6 | Remineralization and export flux. a–f, Time series of main biogeochemical fluxes and respective ratios expressed in terms of nitrogen and carbon over the AO during the historical (1970–2014) and forecast (2015–2100) periods: integrated remineralization rate (TgN yr⁻¹) (**a**), remineralization efficiency (=remineralization in the upper 100 m/export flux) (**b**), nitrogen (**c**)

and carbon (**e**) export fluxes at 100 m (TgN yr⁻¹, TgC yr⁻¹), and respective nitrogen (**d**) and carbon (**f**) export efficiencies illustrating the 'BCP efficiency' (=export flux/net nitrogen assimilation by phytoplankton; export flux/NPP). Bars on the right represent the contributions of climate change (purple), terrigenous inputs (orange) and the scenario uncertainty (black).

scenarios, the future BCP is projected to be less efficient than today. All BCP metrics indicate a less-efficient BCP, regardless of the choice of emission scenario. The dampening mechanisms are similar to those for climate change (that is, warming and subsequent effects). Following a high-emission scenario would decrease the carbon export and transfer efficiencies by 18 and 2.7% (19 and 3.1%, respectively, for nitrogen; Fig. 2a,b) and DIC$_{REMIN}$ by 3%. In general, the scenario uncertainty is greater than or similar in magnitude to the effects of adding terrigenous inputs but smaller than the climate change effects. These results mean that although our projections are sensitive to the choice of CO$_2$ emission scenario (and terrigenous inputs), climate change is consistently driving a substantial decrease in the efficiency of the BCP across all emission scenarios. Finally, following a low-emission trajectory would prevent a shift towards a biogeochemical state with a net CO$_2$ release into the surface layer (Fig. 5d) and a more severe nutrient limitation in the AO (Fig. 3c).

Implications for the ecosystem and biogeochemical cycles

Despite its small size, the AO contributes disproportionately to the global ocean carbon cycle. While it occupies only 1% of the global ocean volume, our model suggests that it contributes ~6.5% to the global carbon sink by the end of the century. In this study, we project a strong and continuous increase in NPP in the AO due to terrigenous inputs and climate change (through the loss of sea ice and the enhanced light availability). This is the largest projected increase in NPP in the global ocean[5]. The AO also accounts for ~8.5% of the global ocean export flux. This is because polar oceans generally have a more efficient BCP than lower latitudes due to larger phytoplankton and abundant nutrients[50]. In line with previous studies[6,15], we found that nitrogen becomes the new 'bottleneck' for the Arctic BCP, even under increasing terrigenous inputs. This shift towards a more nutrient-limited system is generally

associated with a more 'recycled' system in which respiration processes govern, with large implications for both the ecosystem and biogeochemical cycles.

Indeed, at the surface, nutrient limitation drives a transition towards smaller cell size (Supplementary Fig. 2a,b) and higher C:N ratios in phytoplankton (Supplementary Fig. 3). Smaller-sized phytoplankton can reduce the carbon transfer to higher trophic levels[51], thereby threatening endemic megafauna, already vulnerable due to warming and loss of sea ice[52]. Similar to smaller cell size, increasing C:N ratios can have negative consequences for ecosystems. Changes towards higher C:N ratios generally relate to a nutrient-poorer environment and lower the energy transfer efficiency between trophic levels[53]. We therefore interpret the increasing C:N ratios in phytoplankton and the shift towards smaller phytoplankton as a reduction in 'food quality' for higher trophic levels[54]. Congruently, zooplankton biomass decreases (Supplementary Fig. 2c,d), with faster mortality than growth rates (Fig. 2 and Methods). Such changes should be perceived as an increasingly connected and top-down-regulated food web in line with the ongoing 'borealization' of the AO[55].

Planktonic biomass is increasingly lost to the marine environment as detritus. The subsequent increase in organic matter stocks could potentially increase their sinking to greater depths as part of the BCP. However, the increased organic matter production and accumulation at the surface is outcompeted by enhanced remineralization, thereby attenuating the particulate organic carbon flux to depth. First, respiration rates have indeed been shown to increase more rapidly with warming than carbon fixation by phytoplankton[56] and grazing by zooplankton[57]. Second, mesopelagic remineralization by heterotrophic bacteria is expected to increase with both warming and larger organic matter stocks[58]. Consequently, although the AO is projected to double its NPP by the end of the century, it will lose its efficiency to transfer excess carbon and nitrogen to the ocean interior. Instead, the organic

carbon will be more remineralized and added to the growing DIC pool at the surface that will eventually favour outgassing or dampen the chemical buffering capacity. This is best illustrated by the fact that carbon originated from land reduces the AO's carbon sink by up to 10%. Remineralization increases at a fast pace, in particular in the central Arctic (Supplementary Fig. 7), which also poses two potential threats to marine life in the meso- and bathypelagic realms[59]. First, less organic matter (that is, food) from the surface reaches the deep ocean due to the decrease in export and transfer efficiency. Second, enhanced respiration processes exacerbate the emerging concern of deoxygenation, to which the AO is already particularly vulnerable[58] (Extended Data Fig. 2b). Both effects can have negative consequences for life in the deep ocean and on and within the seafloor.

Finally, we want to emphasize the importance of including terrigenous inputs while conducting further Earth system modelling research. We also stress the need to reduce the high uncertainties in contemporary biogeochemical models[60], especially with respect to the land-to-ocean continuum, the fate and degradation of the organic matter from coastal erosion[61–63], the shelf sea dynamics, as well as the parameterizations of grazing[64] and remineralization[65]. Those areas of focus are crucial for refining and enhancing the accuracy of our models in capturing the complexities of ecosystem and biogeochemical cycles[66] in the Arctic and in the global ocean. In this study, acknowledging intrinsic limitations of contemporary biogeochemical models (Methods), we project an overall intensification of marine biogeochemical processes, particularly remineralization. The intensification of remineralization fuels the prevalence of a positive feedback loop over a negative one and slows down biological CO_2 drawdown as well as the export, sequestration and storage of organic carbon. Climate change leads to a counterintuitive 40% reduction in the efficiency of the AO's BCP by 2100, to which terrigenous inputs contribute 10%.

Online content

Any methods, additional references, Nature Portfolio reporting summaries, source data, extended data, supplementary information, acknowledgements, peer review information; details of author contributions and competing interests; and statements of data and code availability are available at https://doi.org/10.1038/s41558-024-02233-6.

References

1. IPCC. in *IPCC Special Report on the Ocean and Cryosphere in a Changing Climate* (eds Pörtner, H. O. et al.) 677–702 (Cambridge Univ. Press, 2019).
2. Lewis, K. M., van Dijken, G. L. & Arrigo, K. R. Changes in phytoplankton concentration now drive increased Arctic Ocean primary production. *Science* **369**, 198–202 (2020).
3. Shu, Q. et al. Arctic Ocean amplification in a warming climate in CMIP6 models. *Sci. Adv.* **8**, eabn9755 (2022).
4. Fox-Kemper, B. et al. in *Climate Change 2021: The Physical Science Basis* (eds Masson-Delmotte, V. et al.) 1211–1362 (IPCC, Cambridge Univ. Press, 2021).
5. Tagliabue, A. et al. Persistent uncertainties in ocean net primary production climate change projections at regional scales raise challenges for assessing impacts on ecosystem services. *Front. Clim.* **3**, 738224 (2021).
6. Tremblay, J. É. et al. Global and regional drivers of nutrient supply, primary production and CO_2 drawdown in the changing Arctic Ocean. *Prog. Oceanogr.* **139**, 171–196 (2015).
7. Turetsky, M. R. et al. Carbon release through abrupt permafrost thaw. *Nat. Geosci.* **13**, 138–143 (2020).
8. Schuur, E. A. G. et al. Permafrost and climate change: carbon cycle feedbacks from the warming arctic. *Annu. Rev. Environ. Resour.* **47**, 343–371 (2022).
9. Strauss, J. et al. A globally relevant stock of soil nitrogen in the Yedoma permafrost domain. *Nat. Commun.* **13**, 6074 (2022).
10. Fritz, M., Vonk, J. E. & Lantuit, H. Collapsing Arctic coastlines. *Nat. Clim. Change* **7**, 6–7 (2017).
11. Nielsen, D. M. et al. Increase in Arctic coastal erosion and its sensitivity to warming in the twenty-first century. *Nat. Clim. Change* **12**, 263–270 (2022).
12. Feng, D. et al. Recent changes to Arctic river discharge. *Nat. Commun.* **12**, 6917 (2021).
13. Zhang, S.-M. et al. Export of nutrients and suspended solids from major Arctic rivers and their response to permafrost degradation. *Adv. Clim. Change Res.* **12**, 466–474 (2021).
14. Terhaar, J., Lauerwald, R., Regnier, P., Gruber, N. & Bopp, L. Around one third of current Arctic Ocean primary production sustained by rivers and coastal erosion. *Nat. Commun.* **12**, 169 (2021).
15. Oziel, L., Schourup-Kristensen, V., Wekerle, C. & Hauck, J. The pan-Arctic continental slope as an intensifying conveyer belt for nutrients in the central Arctic Ocean (1985–2015). *Glob. Biogeochem. Cycles* **36**, e2021GB007268 (2022).
16. Volk, T. & Hoffert, M. I. in *The Carbon Cycle and Atmospheric CO_2: Natural Variations Archean to Present* (eds Sundquist, E. T. & Broecker, W. S.) 99–110 (American Geophysical Union (AGU), 1985).
17. Iversen, M. H. Carbon export in the ocean: a biologist's perspective. *Annu. Rev. Mar. Sci.* **15**, 357–381 (2023).
18. Frenger, I. et al. Misconceptions of the marine biological carbon pump in a changing climate: thinking outside the 'export' box. *Glob. Change Biol.* **30**, e17124 (2024).
19. Rudels, B., Anderson, L. G. & Jones, E. P. Formation and evolution of the surface mixed layer and halocline of the Arctic Ocean. *J. Geophys. Res. Oceans* **101**, 8807–8821 (1996).
20. Carmack, E. & McLaughlin, F. Towards recognition of physical and geochemical change in subarctic and Arctic seas. *Prog. Oceanogr.* **90**, 90–104 (2011).
21. Rainville, L., Lee, C. & Woodgate, R. Impact of wind-driven mixing in the Arctic Ocean. *Oceanography* **24**, 136–145 (2011).
22. Omand, M. M., Govindarajan, R., He, J. & Mahadevan, A. Sinking flux of particulate organic matter in the oceans: sensitivity to particle characteristics. *Sci. Rep.* **10**, 5582 (2020).
23. Regaudie-de-Gioux, A. & Duarte, C. M. Temperature dependence of planktonic metabolism in the ocean. *Glob. Biogeochem. Cycles* **26**, GB1015 (2012).
24. Marsay, C. M. et al. Attenuation of sinking particulate organic carbon flux through the mesopelagic ocean. *Proc. Natl Acad. Sci. USA* **112**, 1089–1094 (2015).
25. Iversen, M. H. & Ploug, H. Temperature effects on carbon-specific respiration rate and sinking velocity of diatom aggregates – potential implications for deep ocean export processes. *Biogeosciences* **10**, 4073–4085 (2013).
26. Le Moigne, F. A. C. et al. Carbon export efficiency and phytoplankton community composition in the Atlantic sector of the Arctic Ocean. *J. Geophys. Res. Oceans* **120**, 3896–3912 (2015).
27. Henson, S., Le Moigne, F. & Giering, S. Drivers of carbon export efficiency in the global ocean. *Glob. Biogeochem. Cycles* **33**, 891–903 (2019).
28. Kwon, E. Y., Primeau, F. & Sarmiento, J. L. The impact of remineralization depth on the air–sea carbon balance. *Nat. Geosci.* **2**, 630–635 (2009).
29. Buesseler, K. O., Boyd, P. W., Black, E. E. & Siegel, D. A. Metrics that matter for assessing the ocean biological carbon pump. *Proc. Natl Acad. Sci. USA* **117**, 9679–9687 (2020).
30. Hauck, J. & Völker, C. Rising atmospheric CO_2 leads to large impact of biology on Southern Ocean CO_2 uptake via changes of the Revelle factor. *Geophys. Res. Lett.* **42**, 1459–1464 (2015).
31. Gürses, Ö. et al. Ocean biogeochemistry in the coupled ocean–sea ice–biogeochemistry model FESOM2.1–REcoM3. *Geosci. Model Dev.* **16**, 4883–4936 (2023).

32. O'Neill, B. C. et al. The Scenario Model Intercomparison Project (ScenarioMIP) for CMIP6. *Geosci. Model Dev.* **9**, 3461–3482 (2016).

33. Babin, M. Climate change tweaks Arctic marine ecosystems. *Science* **369**, 137–138 (2020).

34. Kim, Y.-H., Min, S.-K., Gillett, N. P., Notz, D. & Malinina, E. Observationally-constrained projections of an ice-free Arctic even under a low emission scenario. *Nat. Commun.* **14**, 3139 (2023).

35. Lim, H.-G., Kug, J.-S. & Park, J.-Y. Biogeophysical feedback of phytoplankton on Arctic climate. Part II: Arctic warming amplified by interactive chlorophyll under greenhouse warming. *Clim. Dyn.* **53**, 3167–3180 (2019).

36. Timmermans, M. & Marshall, J. Understanding Arctic Ocean circulation: a review of ocean dynamics in a changing climate. *J. Geophys. Res. Oceans* **125**, e2018JC014378 (2020).

37. Muilwijk, M. et al. Divergence in climate model projections of future Arctic Atlantification. *J. Clim.* **36**, 1727–1748 (2023).

38. Li, W. K. W., McLaughlin, F. A., Lovejoy, C. & Carmack, E. C. Smallest algae thrive as the Arctic ocean freshens. *Science* **326**, 539 (2009).

39. Hoppe, C. J. M., Wolf, K. K. E., Schuback, N., Tortell, P. D. & Rost, B. Compensation of ocean acidification effects in Arctic phytoplankton assemblages. *Nat. Clim. Change* **8**, 529–533 (2018).

40. Yasunaka, S. et al. An assessment of CO_2 uptake in the Arctic Ocean from 1985 to 2018. *Glob. Biogeochem. Cycles* **37**, e2023GB007806 (2023).

41. Revelle, R. & Suess, H. E. Carbon dioxide exchange between atmosphere and ocean and the question of an increase of atmospheric CO_2 during the past decades. *Tellus* **9**, 18–27 (1957).

42. Lotze, H. K. et al. Global ensemble projections reveal trophic amplification of ocean biomass declines with climate change. *Proc. Natl Acad. Sci. USA* **116**, 12907–12912 (2019).

43. Bruhn, A. D. et al. Terrestrial dissolved organic matter mobilized from eroding permafrost controls microbial community composition and growth in arctic coastal zones. *Front. Earth Sci.* **9** (2021).

44. Mann, P. J. et al. Degrading permafrost river catchments and their impact on Arctic Ocean nearshore processes. *Ambio* **51**, 439–455 (2022).

45. Kim, H. H., Laufkötter, C., Lovato, T., Doney, S. C. & Ducklow, H. W. Projected 21st-century changes in marine heterotrophic bacteria under climate change. *Front. Microbiol.* **14**, 1049579 (2023).

46. McDonnell, A. M. P., Boyd, P. W. & Buesseler, K. O. Effects of sinking velocities and microbial respiration rates on the attenuation of particulate carbon fluxes through the mesopelagic zone: sinking, respiration, and flux attenuation. *Glob. Biogeochem. Cycles* **29**, 175–193 (2015).

47. Crippa, M. et al. *Fossil CO_2 Emissions of All World Countries - 2020 Report* (Publications Office of the European Union, 2022).

48. Polimene, L. et al. Biological lability of terrestrial DOM increases CO_2 outgassing across Arctic shelves. *Biogeochemistry* **160**, 289–300 (2022).

49. Bertin, C. et al. Biogeochemical river runoff drives intense coastal Arctic Ocean CO_2 outgassing. *Geophys. Res. Lett.* **50**, e2022GL102377 (2023).

50. Siegel, D. A., DeVries, T., Cetinic, I. & Bisson, K. M. Quantifying the Ocean's biological pump and its carbon cycle impacts on global scales. *Annu. Rev. Mar. Sci.* **15**, 329–356 (2023).

51. Wiedmann, I. et al. Arctic observations identify phytoplankton community composition as driver of carbon flux attenuation. *Geophys. Res. Lett.* **47**, e2020GL087465 (2020).

52. Wassmann, P. Arctic marine ecosystems in an era of rapid climate change. *Prog. Oceanogr.* **90**, 1–17 (2011).

53. Dickman, E. M., Newell, J. M., González, M. J. & Vanni, M. J. Light, nutrients, and food-chain length constrain planktonic energy transfer efficiency across multiple trophic levels. *Proc. Natl Acad. Sci. USA* **105**, 18408–18412 (2008).

54. Kwiatkowski, L., Aumont, O., Bopp, L. & Ciais, P. The impact of variable phytoplankton stoichiometry on projections of primary production, food quality, and carbon uptake in the global ocean. *Glob. Biogeochem. Cycles* **32**, 516–528 (2018).

55. Ingvaldsen, R. B. et al. Physical manifestations and ecological implications of Arctic Atlantification. *Nat. Rev. Earth Environ.* **2**, 874–889 (2021).

56. Leles, S. G. & Levine, N. M. Mechanistic constraints on the trade-off between photosynthesis and respiration in response to warming. *Sci. Adv.* **9**, eadh8043 (2023).

57. Steinberg, D. K. & Landry, M. R. Zooplankton and the ocean carbon cycle. *Annu. Rev. Mar. Sci.* **9**, 413–444 (2017).

58. Kwiatkowski, L. et al. Twenty-first century ocean warming, acidification, deoxygenation, and upper-ocean nutrient and primary production decline from CMIP6 model projections. *Biogeosciences* **17**, 3439–3470 (2020).

59. Martin, A. et al. The oceans' twilight zone must be studied now, before it is too late. *Nature* **580**, 26–28 (2020).

60. Henson, S. A. et al. Uncertain response of ocean biological carbon export in a changing world. *Nat. Geosci.* **15**, 248–254 (2022).

61. Vonk, J. E. et al. Preferential burial of permafrost-derived organic carbon in Siberian-Arctic shelf waters. *J. Geophys. Res. Oceans* **119**, 8410–8421 (2014).

62. Martens, J., Wild, B., Semiletov, I., Dudarev, O. V. & Gustafsson, Ö. Circum-Arctic release of terrestrial carbon varies between regions and sources. *Nat. Commun.* **13**, 5858 (2022).

63. Tanski, G. et al. Rapid CO_2 release from eroding permafrost in seawater. *Geophys. Res. Lett.* **46**, 11244–11252 (2019).

64. Rohr, T., Richardson, A. J., Lenton, A., Chamberlain, M. A. & Shadwick, E. H. Zooplankton grazing is the largest source of uncertainty for marine carbon cycling in CMIP6 models. *Commun. Earth Environ.* **4**, 212 (2023).

65. del Giorgio, P. A. & Duarte, C. M. Respiration in the open ocean. *Nature* **420**, 379–384 (2002).

66. Burd, A. B. Modeling the vertical flux of organic carbon in the global ocean. *Annu. Rev. Mar. Sci.* **16**, 135–161 (2024).

Methods

Definitions, concepts and metrics for the BCP

Biological carbon pump. In this study, we focus on the 'soft-tissue' pump, that is, the suite of processes that mediate transport of particulate organic carbon from the surface to the deeper ocean. This organic carbon is subsequently decomposed back to DIC (the sum of CO_2, HCO_3^- and CO_3^{2-}) and thus contributes to enriching the deep ocean reservoir with DIC. By doing so, the BCP isolates ocean carbon from contact with the atmosphere and helps to reduce the atmospheric CO_2 concentration. The reader is referred to reviews such as those of refs. [17,50].

Export flux. This is the amount of (particulate) organic carbon (or nitrogen) that sinks out of the euphotic zone (typically 100 m below the base of the euphotic zone), also referred to as 'export production'.

Export efficiency. This is the capacity of the ocean to export organic matter produced at the surface. Mathematically, this is the exported fraction of NPP (=export flux/NPP), also commonly defined as the ratio of export flux to the depth-integrated NPP.

Remineralization. This pertains to respiration processes that convert organic matter (both particulate and dissolved) into inorganic compounds, typically referred to as dissolved inorganic carbon and nutrients. This process causes an attenuation of organic carbon and other elemental fluxes, that is, a decrease in fluxes with increasing depth. In this study, we implicitly consider that remineralization is bacterial, affecting both carbon and nitrogen. We consider plankton respiration separately because it only affects carbon.

Remineralization efficiency. This is the ability of the ocean to attenuate the export flux through remineralization. It is the ratio between the remineralization rate in the upper 100 m and the export flux.

Biologically driven p_{CO_2} changes at the surface ocean. This is an indicator for the proportion of the seawater p_{CO_2} that is either removed from the surface ocean layer or added to the surface ocean layer due to biological activity. It depends on the balance between carbon fixation, respiratory processes and the buffer factor (γ_{DIC}, see Revelle factor). It is calculated seasonally following ref. [30] as $\frac{\Delta DIC \times p_{CO_2}}{\gamma_{DIC}}$. ΔDIC is the carbon drawdown by biological production in the top 100 m layer of the ocean (=gross primary production minus remineralization minus respiration).

Sequestration flux. This is the amount of (particulate) organic carbon (or nitrogen) that sinks out below 600 m that is thus removed from exchange with the atmosphere on a long timescale.

Transfer efficiency. This is the capacity of the ocean to sequester organic matter. The transfer efficiency is the ratio between the sequestration flux in the deep ocean at 600 m and the export flux at 100 m (for carbon or nitrogen), which measures the efficiency to sequester carbon for centuries to millennia.

DIC_{REMIN}. This is an indicator for the storage of carbon of biological origin in the ocean interior[18] and thus, the BCP. It is calculated from the apparent oxygen utilization (AOU). AOU is a measure of the difference between the observed oxygen concentration and the oxygen concentration at saturation, with $DIC_{REMIN} = r$ AOU $= r$ ($O_{2_{SAT}} - O_2$), and $r = C:O = 0.688$. In this study, DIC_{REMIN} is integrated for depth greater than 100 m. It offers an integrative view of the BCP by considering the balance between the 'gain side' (export flux) but also the 'loss side' through oceanic circulation.

BCP efficiency. This refers to the capacity of the BCP to export, sequester and store carbon that is produced in the surface layer. The BCP efficiency is assessed through the combination of four metrics: biologically driven p_{CO_2} changes, the export and transfer efficiencies, and DIC_{REMIN}.

Revelle factor. This is an indicator of the chemical 'buffering' capacity of the surface ocean. The Revelle factor is the ratio of the relative change in seawater p_{CO_2} to the relative change in DIC[67,68]. It varies between 8 in warm and 15 in cold waters in the historical period[69]. The lower the Revelle factor, the more efficient is the anthropogenic CO_2 uptake[70]. As the ocean continues to take up CO_2, the carbonate system is pushed towards higher CO_2 concentrations and the Revelle factor increases[67]. Consequently, the buffer capacity of the ocean and its CO_2 uptake capacity decrease. This positive feedback limits the increase in the ocean CO_2 sink in the future[71]. The Revelle factor and buffer factors (R and γ_{DIC}) are linked via the relation $\gamma_{DIC} = DIC/R$ and can be derived from the carbonate system parameters[68]. Here we calculated them offline using mocsy routines (v.2.0)[72]. We note that the exact same code was used online to model the ocean carbonate system.

Study area

In this study, we defined the AO as the area roughly north of 66.5° N. It encompasses 11 Arctic regions: Barents Sea, Kara Sea, Laptev Sea, East Siberian Sea, Chukchi Sea, Beaufort Sea, Canadian Archipelago, Baffin Bay, Nordic Seas, and the Eurasian and Amerasian basins (Extended Data Fig. 1).

FESOM-REcoM model description

We used the Finite VolumE Sea ice-Ocean Model v.2.1 (FESOM2.1). FESOM is a global ocean circulation model using an unstructured mesh, which includes a dynamic-thermodynamic sea ice model[73–75]. FESOM has been developed for more than two decades and this version has been specifically assessed and tuned for the Arctic Ocean in single-model studies[76,77], in Model Intercomparison Projects[3,78–82], and included in the AWI (Alfred Wegener Institute, Germany) Climate Model[83,84]. Coupled to FESOM2.1 is the Regulated Ecosystem Model v.3 (REcoM3), a 'state-of-the-art' biogeochemical model of intermediate complexity[85]. REcoM3 resolves the biogeochemical fluxes of carbon, nitrogen, silicon, iron and oxygen with a total of 28 prognostic tracers including the full carbonate chemistry and air–sea CO_2 exchange using the mocsy 2.0 scheme[72]. REcoM, which has been developed for the past 18 years[86], has been extensively evaluated: (1) in multimodel ensemble studies for the global ocean[87–90] and the Arctic Ocean[40]; and (2) in single-model global[91–93] and Arctic Ocean studies[94–97]. REcoM has also been successfully used to make future projections[98–101]. For a detailed description and skill assessment of the latest version used in this study, we refer to ref. [31] and to the Supplementary Information. Another strength of REcoM3 lies in its flexible stoichiometry, which allows variations in elemental composition, and therefore differs from many models that use stoichiometry fixed at the Redfield ratio. Flexible stoichiometry is a more realistic representation of nature since, for example, the C:N stoichiometry of phytoplankton and organic matter has been shown to exhibit considerable spatiotemporal deviations from the Redfield ratio in measurements[102] and in this study.

Model setup and simulations

For this study, we used a global mesh with enhanced horizontal resolution of 4.5 km at the pan-Arctic scale[94,96,103], referred to as 'fArc'. At the ocean surface, we forced the model with output from the AWI Climate Model (AWI-CM[83]) produced for the CMIP6. Therefore, the atmospheric forcing encompasses physical ocean–atmosphere feedback while not reflecting ocean biogeochemistry feedback on the atmosphere. We used 3-hourly output of winds, near-surface air temperature and humidity, downward shortwave and longwave radiation fluxes, and freshwater fluxes and daily output of terrestrial freshwater run-off from the first ensemble member of the historical simulation until 2014,

and the SSP1-2.6, SSP2-4.5, SSP3-7.0 and SSP5-8.5 scenario simulations thereafter. In agreement with the literature, we found that discharge from Arctic rivers is expected to increase in the future[12,81]. Atmospheric p_{CO_2} levels are taken from ref. 104 for the historical period 1950–2014 and from ref. 32 for the period 2015–2100, consistent with the time series used in the CMIP6 experiments.

We first spun up FESOM2.1-REcoM3 for 50 years (4 times the 1950–1959 period and then once the 1950–1969 period; Extended Data Table 1). We first ran a control run, allowing for an assessment of model drift (Extended Data Fig. 3) by repeating the atmospheric conditions of the 1950 decade (1950–1959) and atmospheric p_{CO_2} typical for 1950 (312.82 ppm). Looping over a decade instead of a single year aims to minimize the effect of natural climate oscillations such as the North Atlantic or Arctic Oscillations. All remaining simulations are transient, that is, performed with varying climate and atmospheric CO_2. We ran two historical runs (1970–2014): one with and one without terrigenous inputs (including river and coastal erosion) denoted Terr and noTerr, respectively. Then, we ran five main forecast experiments for the years 2015–2100. First, we ran the four scenarios (SSP1-2.6, SSP2-4.6, SSP3-7.0 and SSP5-8.5) with terrigenous inputs, which were branched off the historical simulation with terrigenous inputs. We chose the high-emission scenario SSP3-7.0 as our baseline simulation because the most plausible scenarios are between SSP2-4.5 and SSP3-7.0. SSP5-8.5 is considered highly unlikely[105]. Subsequently, we ran a reference simulation without terrigenous inputs (SSP3-7.0) branched off the historical simulation without terrigenous inputs. Finally, we ran four additional historical simulations: two attributing erosion-derived inputs to different pools (dissolved or particulate organic matter), one using a more advanced parametrization of particle sinking speed and remineralization following ref. 106, and one without coloured dissolved organic matter (CDOM) absorption.

Implementation of terrigenous inputs

We implemented a dynamically coupled (monthly and yearly varying) parametrization of riverine and erosion inputs of carbon and nutrients (for the area North of 60° N) based on the climatological monthly resolved observational dataset provided by ref. 14. The dataset provides river fluxes of total alkalinity, dissolved inorganic carbon, dissolved organic carbon, dissolved inorganic nitrogen, dissolved organic nitrogen and silicic acid. It also provides coastal erosion inputs expressed in total carbon and nitrogen. Note that silicic acid is not documented in the erosion dataset and is scaled in this study with total dissolved nitrogen on the basis of a fixed N:Si ratio of ~9 found in rivers at pan-Arctic scale following ref. 107. Terrigenous inputs do not take into account glacier discharge and subsea permafrost, although it is acknowledged that they can both provide important quantities of carbon and nutrients[108–111]. We therefore consider our estimates of terrigenous inputs to be conservative.

As the erosion inputs are expressed in total carbon and nitrogen, and do not specify the pool (particulate or dissolved, organic or inorganic), we used the same protocol as that in ref. 14: we attributed the erosion inputs to the dissolved inorganic pool (that is, instantly remineralized). This choice and assumption was evaluated with a sensitivity test and is discussed in the section 'Fate of organic matter'. We scaled the annual riverine and coastal erosion inputs, expressed in total mass (Tg) of the chemical compound, to the annual freshwater river discharge and air temperature anomalies (provided by the forcing AWI-CM), respectively, with the reference period considered as the 1970–1990 period (Fig. 1a,b and Supplementary Information). We also included CDOM light attenuation on the basis of the ratio between dissolved organic carbon (DOC) and CDOM estimated empirically from ocean-colour remote sensing[112].

CMIP6 comparison

To evaluate whether or not our single-model results were consistent with other modern Earth system models, we derived the export and

remineralization efficiencies from the CMIP6 ensemble, for historical and all emission scenarios (SSP1-2.6, SSP2-4.5, SSP3-7.0, SSP5-8.5). The CMIP6 ensemble showed very similar dynamics as our model. In a first analysis (Extended Data Fig. 4), using 16 (ACCESS-ESM1-5, CanESM5-1, CanESM5-CanOE, CanESM5, CESM2, CESM2-WACCM, CNRM-ESM2-1, GFDL-ESM4, IPSL-CM5A2-INCA, IPSL-CM6A-LR, MIROC-ES2L, MPI-ESM1-2-HR, MPI-ESM1-2-LR, NorESM2-LM, NorESM2-MM, UKESM1-0-LL) to 17 (plus MRI-ESM2-0) CMIP6 Earth System Models depending on the emission scenarios, we demonstrated dynamics consistent with our model results. The ensemble provides a robust increase in NPP in line with ref. 58, and an inflection point for the export flux occurring in the first half of the twenty-first century. In a second analysis (Extended Data Fig. 5), we also showed a robust decreasing export efficiency and increasing remineralization efficiency, independently of the choice of emission scenario. However, this last analysis was limited to five models (CESM2, CESM2-WACCM, IPSL-CM6A-LR, MPI-ESM1-2-HR, MPI-ESM1-2-LR) because only few models provide remineralization outputs. The biogeochemical components of those Earth System models have been extensively documented and described in the literature (for more detailed descriptions, see refs. 58,113,114).

Evaluation of model skills, limitations and uncertainties

Net primary production. This 'Arctic-adapted' model configuration was tuned to achieve realistic NPP levels (Supplementary Figs. 10 and 11). To this end, we evaluated the model historical simulation (Terr) by comparing with 'state-of-the-art' ocean-colour products from Stanford ('Arctic-tuned'[2,115]) and from Copernicus-GlobColour ('global ocean', product ID: OCEANCOLOUR_GLO_BGC_L4_MY_009_104), thereby updating the previous assessment[14], which used the outdated dataset from ref. 116. On the basis of in situ observations, the 'Stanford' dataset by refs. 2,115 corrected artefacts due to coloured dissolved organic matter and non-algal particles, especially on the Russian shelves. This led to much lower remotely sensed NPP estimates (310–370 TgC; Supplementary Table 1), while the previous dataset from ref. 116 yielded 540 TgC yr⁻¹. The global dataset from Globcolour provided an estimate of 369 TgC yr⁻¹. Our estimations of absolute NPP of 509 TgC yr⁻¹ were consistent with the 551 TgC yr⁻¹ obtained by ref. 14 over the same study area and time period (2005–2010). When comparing Terr with the 'Stanford' dataset in the $\log_{10}$ space, we found the following statistics: correlation coefficient $R = 0.86$, root mean square error (RMSE) = 0.4 ± 0.43 gC m⁻² yr⁻¹ (s.d.). We argue that modelled depth-integrated NPP is greater than remotely sensed NPP because satellites only assess the surface layer in open waters, whereas the model considers the whole water column and also considers ice-covered areas, which can notably contribute to pelagic production[117–119]. In terms of nitrate assimilation[2], we estimated (on the basis of a constant C:N ratio) annual values of 58.2 TgN yr⁻¹, while our flexible stoichiometry model yielded lower values of 31.7 TgN yr⁻¹. Our results differed in the terrigenous-driven relative increase in NPP compared with ref. 14. We found that NPP increased by 16% with terrigenous inputs, whereas ref. 14 found the increase to be 28% (2005–2010). In our simulations, we reached a 21% relative increase in NPP due to terrigenous inputs only by 2100 (SSP3-7.0). If we consider nitrogen instead of carbon for assessing the increased phytoplankton production, the terrigenous-driven relative increase reaches 33% (Fig. 2). Such differences can arise from different formulations between general ocean circulation and biogeochemical models, in particular those related to remineralization, recycling and stoichiometry.

Fate of organic matter. At the pan-Arctic scale, simulated total remineralization due to terrigenous inputs amounts to 7.9 TgN yr⁻¹ (Extended Data Table 2), largely exceeding the actual terrigenous inputs of nitrogen used as forcing, which accounted for ~2.6 TgN yr⁻¹. This 'amplification' effect supports the idea of a positive feedback loop. Reference 14 also found that 2.6 TgN yr⁻¹ of terrigenous inputs (equivalent to

17 TgC yr^{-1} with constant C:N ratio of 122:16) were responsible for an NPP increase of 140 TgC yr^{-1}, suggesting that terrigenous inputs are recycled more than 8 times before they are out of reach for primary producers (either exported to depth, buried in sediments or transported out of the AO). By comparison, we found that the same 2.6 TgN yr^{-1} drove an increase of 5.2 TgN yr^{-1} in net nitrogen assimilation (using EXP-2 for exactly the same time period and studied area), suggesting that in our model, terrigenous inputs are recycled only 2 times before they are out of reach for primary producers. The disparities between the two models may be attributed to either insufficient remineralization in our model and/or insufficient lateral transport in their model. In both models, remineralization is driven by temperature through similar functions (Q10 both in REcoM and in PISCES used by ref. 14). But we also argue that this discrepancy between the model experiments is exacerbated by the fact that they used a rather short spin up time (15 years compared with 50 years in our study), which may not be sufficient to observe long-term feedback and to reach equilibrium in the mesopelagic layer in the model. In addition, by using a fixed stoichiometry model, they probably overestimate the effect of terrigenous inputs on NPP in a context of increasing C:N ratios.

We acknowledge the high uncertainties related to the fate of the organic matter released from permafrost[61–63]. However, several studies showed that thawing permafrost in soils of coastal areas release one of the most labile forms of organic matter in nature[44,120–122]. Furthermore, Arctic shelves exhibit strong remineralization rates of terrigenous organic matter in the Laptev Sea and East Siberian Sea, being 0.87 TgN yr^{-1} in sediments and 0.38 TgN yr^{-1} in the water column[123,124]. In the same areas, our model experiments indicated a much larger benthic and water column remineralization that reached 2.43 and 1.5 TgN yr^{-1}, respectively.

We here evaluate our choice of remineralizing instantaneously the carbon and nitrogen that originated from the thawing permafrost responsible for the coastal erosion. To do so, we ran two additional historical runs (1970–2014) with erosion-originated carbon and nitrogen put into the dissolved organic pools (EXP-7) or into the particulate organic pools (EXP-8), instead of the dissolved inorganic pools (Terr, baseline, EXP-3; Extended Data Table 1). We found that routing coastal erosion carbon and nutrients towards the dissolved organic pool instead of the inorganic pool (EXP-7 minus EXP-3) surprisingly resulted in more NPP (+48 TgC, +9.4%) and export flux (+11 TgC, +20%), slightly more CO$_2$ uptake and less outgassing by about −5% (−9 TgC; Supplementary Table 2). Routing coastal erosion to the particulate pool also resulted in an increase in NPP (+23 TgC, +4.5%) and export flux (+5.5 TgC, +10%), but to a smaller extent. In contrast to EXP-7, EXP-8 resulted in more outgassing (+20 TgC, +11%). All experiments remain in the range of previous modelled or observational studies. The reader is referred to the next section for more details on the model simulation skills to represent Arctic CO$_2$ fluxes. We found that the remineralization and export efficiencies showed very small deviations from the baseline simulation in EXP-7 and EXP-8 (Supplementary Fig. 12), and they remained relatively constant during the historical period. Thus, while the selection of a specific destination pool for coastal erosion could lead to variations of up to 20% in NPP and export fluxes, our investigations unveiled that the underlying mechanisms, as elucidated in this study, remained consistent regardless of this choice. However, a more realistic separation of the destination pools is needed to better estimate Arctic Ocean biogeochemical fluxes.

We acknowledge additional limitations of the model regarding the representation of dissolved organic matter (DOM) lability. We only consider semi-labile DOM, although we know that terrigenous and oceanic-originated organic matter can have different lability[48,125]. Terrigenous matter forms a large fraction of the organic matter on the Siberian shelves and was assumed to be largely refractory on the basis of almost conservative mixing behaviour[126–128]; newer studies, however, have shown that a large fraction (more than 70%[129]) is

labile[128–130], with degradation timescales in the semi-labile continuum. However, a small fraction of the carbon that is consumed by microbes can contribute to the refractory DOM pool that cycles on timescales of thousands of years[131,132]. A key question is whether the Arctic DOC inventory increases as a result of the increased microbial turnover, similar to recent observation in freshwater environments on land[133]. Currently, the major fraction of terrigenous DOC (>50% of annual flux) is exported during the freshet[107] and originates from modern plant litter that is less labile compared with old organic carbon mobilized from thawing permafrost. With amplifying Arctic warming, the fraction of labile organic carbon from thawing and eroding permafrost potentially increases. Moreover, we do not consider photodegradation[134]. The importance of photodegradation in the Arctic is poorly known. However, there are indications that high turbidity and absorption, especially in river-influenced coastal and shelf waters, limits photodegradation[135,136].

The absence of burial in the model potentially biases our results and may cause slightly overestimated NPP levels. Total burial of organic carbon in the Arctic (excluding the Bering strait/Chukchi shelf and the Canadian Archipelago, for which a comprehensive budget was not possible) has been estimated at a bit less than 10 TgC yr^{-1} (ref. 137). Most of that burial derives from the terrestrial (allochthonous) particulate OM input, with high C:N ratio and a large negative value of Δ^{13}C, of which roughly half stems from coastal erosion. We can roughly estimate the error in our model input fluxes in the following way, by assuming equal lability of riverine and permafrost OM: the burial probability of terrestrial-originated particulate OM is roughly 10/14 (ref. 137). Total input of particulate OM from coastal erosion from the same source is ~7 TgC yr^{-1}. Of this input, therefore ~7 × 10/14 = 5 TgC yr^{-1} might get buried. We might therefore overestimate the erosion input by the same amount as we are inputting a total amount of carbon of 15.4 TgC yr^{-1} from coastal erosion[14]. On the other hand, we have not included particulate OM in our model riverine inputs. Of the ~7 TgC yr^{-1} estimated in ref. 137, ~4/14 get remineralized in the water column and sediment, which would amount to an underestimate of the effective riverine OM input by ~2 TgC yr^{-1}. A higher lability of permafrost-derived (erosion) particulate OM than that of riverine particulate OM would reduce both absolute numbers, which would further balance out the remaining 3 TgC yr^{-1}. The absence of burial is also somehow compensated by the carbon and nitrogen accumulation in the sediment (Supplementary Fig. 13) and by the fact we introduced a loss term for nitrogen in the sediment through benthic denitrification.

Export flux. The export flux was evaluated for both the Arctic Ocean and the global ocean at many different depths using the most comprehensive current observational dataset for the sinking of particulate organic matter[138] (Supplementary Fig. 14). We found that the modelled export flux was able to reproduce observations significantly (with doubled-sided t-test P values < 0.001) and reasonably well on a global scale ($r = 0.21$) and with a noticeable improvement for the Arctic Ocean ($r = 0.39$). Note that the statistics were derived from non-log-transformed data.

CO$_2$ fluxes. Here we consider negative (positive) fluxes to be CO$_2$ uptake (outgassing) by the ocean. Estimated fluxes from our simulation (Terr) are -140.5 ± 4.2 TgC yr^{-1}, while the Regional Carbon Cycle Assessment and Processes project, phase 2 (RECCAP2, https://www.globalcarbonproject.org/reccap/) documented -116 ± 4 TgC yr^{-1} from observation-based p_{CO_2} products and -92 ± 30 TgC yr^{-1} from the ensemble mean of global ocean biogeochemistry models[40]. For this RECCAP2 calculation to be comparable, we used the exact same 1985–2018 time period and mask (https://github.com/RECCAP2-ocean/R2-shared-resources/blob/master/data/regions/RECCAP2_region_masks_all_v20221025.nc). The RECCAP2 assessment is the latest and most comprehensive assessment of the Arctic Ocean CO$_2$ uptake,

yet uncertainties are probably larger than reported standard deviations. This is because surface ocean CO_2 observations that form the basis of observation-based estimates and are the first-order evaluation metric for the ocean biogeochemistry models are still sparse in large parts of the Arctic, and particularly in winter[40]. Most of the available data are from the western Greenland Sea, the Beaufort Shelf, the Chukchi Sea and the Barents Sea, while much less data are available for the Central Basin and Siberian shelf seas. Other Arctic-specific model or mass balance studies estimated the AO carbon sink at about −153 ± 14 TgC yr^{-1} (ref. 139) or −166 ± 60 TgC yr^{-1} (ref. 140). Our additional experiments such as EXP-7 and EXP-8 yielded CO_2 fluxes of about −150 TgC yr^{-1} and −120 TgC yr^{-1}, which remain in the range of previous estimations. Our results are thus consistent with previous estimates.

Data availability
The minimal dataset required to reproduce the findings of this study is available on Zenodo at https://doi.org/10.5281/zenodo.14228166 (ref. 141). Model outputs are too large and will be provided upon request to the corresponding author.

Code availability
FESOM and REcoM continue to be further developed and are publicly available under a GNU GPL licence. The Fortran source code of FESOM2.1-REcoM3 can be obtained via https://fesom.de/models/fesom20 (last access 21 September 2024). The custom model code and the post-processing scripts underlying the figures are available on Zenodo at https://doi.org/10.5281/zenodo.14228166 (ref. 141). The analysis of the model output was done with the open-source software Python.

References

67. Zeebe, R. & Wolf-Gladrow, D. *CO₂ in Seawater: Equilibrium, Kinetics, Isotopes* Elsevier Oceanography Book Series 65 (Elsevier Science, 2001).
68. Egleston, E. S., Sabine, C. L. & Morel, F. M. M. Revelle revisited: buffer factors that quantify the response of ocean chemistry to changes in DIC and alkalinity. *Glob. Biogeochem. Cycles* (2010).
69. Broecker, W. S., Takahashi, T., Simpson, H. J. & Peng, T.-H. Fate of fossil fuel carbon dioxide and the Global Carbon Budget. *Science* **206**, 409–418 (1979).
70. Sabine, C. L. et al. The oceanic sink for anthropogenic CO₂. *Science* **305**, 367–371 (2004).
71. Wallace, D. W. R. in *International Geophysics* Vol. 77 (eds Siedler, G. et al.) 489–521 (Academic Press, 2001).
72. Orr, J. C. & Epitalon, J.-M. Improved routines to model the ocean carbonate system: mocsy 2.0. *Geosci. Model Dev.* **8**, 485–499 (2015).
73. Danilov, S., Sidorenko, D., Wang, Q. & Jung, T. The Finite-volumE Sea ice–Ocean Model (FESOM2). *Geosci. Model Dev.* **10**, 765–789 (2017).
74. Scholz, P. et al. Assessment of the Finite-volumE Sea ice–Ocean Model (FESOM2.0) - part 1: description of selected key model elements and comparison to its predecessor version. *Geosci. Model Dev.* **12**, 4875–4899 (2019).
75. Scholz, P. et al. Assessment of the Finite-VolumE Sea ice-Ocean Model (FESOM2.0) - part 2: partial bottom cells, embedded sea ice and vertical mixing library CVMix. *Geosci. Model Dev.* **15**, 335–363 (2022).
76. Li, X. et al. Eddy activity in the Arctic Ocean projected to surge in a warming world. *Nat. Clim. Change* **14**, 156–162 (2024).
77. Wekerle, C. et al. Atlantic Water warming increases melt below Northeast Greenland's last floating ice tongue. *Nat. Commun.* **15**, 1336 (2024).
78. Khosravi, N. et al. The Arctic Ocean in CMIP6 models: biases and projected changes in temperature and salinity. *Earths Future* **10**, e2021EF002282 (2022).
79. Pan, R. et al. Future Arctic climate change in CMIP6 strikingly intensified by NEMO-family climate models. *Geophys. Res. Lett.* **50**, e2022GL102077 (2023).
80. Shu, Q. et al. Arctic Ocean simulations in the CMIP6 Ocean Model Intercomparison Project (OMIP). *Geosci. Model Dev.* **16**, 2539–2563 (2023).
81. Wang, S., Wang, Q., Wang, M., Lohmann, G. & Qiao, F. Arctic Ocean freshwater in CMIP6 coupled models. *Earths Future* **10**, e2022EF002878 (2022).
82. Treguier, A. M. et al. The mixed-layer depth in the Ocean Model Intercomparison Project (OMIP): impact of resolving mesoscale eddies. *Geosci. Model Dev.* **16**, 3849–3872 (2023).
83. Semmler, T. et al. Simulations for CMIP6 with the AWI climate model AWI-CM-1-1. *J. Adv. Model. Earth Syst.* **12**, e2019MS002009 (2020).
84. Streffing, J. et al. AWI-CM3 coupled climate model: description and evaluation experiments for a prototype post-CMIP6 model. *Geosci. Model Dev.* **15**, 6399–6427 (2022).
85. Fennel, K. et al. Ocean biogeochemical modelling. *Nat. Rev. Methods Prim.* **2**, 76 (2022).
86. Schartau, M. et al. Modelling carbon overconsumption and the formation of extracellular particulate organic carbon. *Biogeosciences* **4**, 433–454 (2007).
87. Laufkötter, C. et al. Projected decreases in future marine export production: the role of the carbon flux through the upper ocean ecosystem. *Biogeosciences* **13**, 4023–4047 (2016).
88. Laufkötter, C., John, J. G., Stock, C. A. & Dunne, J. P. Temperature and oxygen dependence of the remineralization of organic matter. *Glob. Biogeochem. Cycles* **31**, 1038–1050 (2017).
89. Hauck, J. et al. Consistency and challenges in the ocean carbon sink estimate for the global carbon budget. *Front. Mar. Sci.* **7**, 571720 (2020).
90. Friedlingstein, P. et al. Global Carbon Budget 2023. *Earth Syst. Sci. Data* **15**, 5301–5369 (2023).
91. Schourup-Kristensen, V., Sidorenko, D., Wolf-Gladrow, D. A. & Völker, C. A skill assessment of the biogeochemical model REcoM2 coupled to the Finite Element Sea Ice–Ocean Model (FESOM 1.3). *Geosci. Model Dev.* **7**, 2769–2802 (2014).
92. Karakuş, O. et al. Modeling the impact of macrozooplankton on carbon export production in the Southern Ocean. *J. Geophys. Res. Oceans* **126**, e2021JC017315 (2021).
93. Karakuş, O., Völker, C., Iversen, M., Hagen, W. & Hauck, J. The role of zooplankton grazing and nutrient recycling for global ocean biogeochemistry and phytoplankton phenology. *J. Geophys. Res. Biogeosci.* **127**, e2022JG006798 (2022).
94. Schourup-Kristensen, V., Wekerle, C., Wolf-Gladrow, D. A. & Völker, C. Arctic Ocean biogeochemistry in the high resolution FESOM 1.4-REcoM2 model. *Prog. Oceanogr.* **168**, 65–81 (2018).
95. Schourup-Kristensen, V., Wekerle, C., Danilov, S. & Völker, C. Seasonality of mesoscale phytoplankton control in eastern Fram strait. *J. Geophys. Res. Oceans* **126**, e2021JC017279 (2021).
96. Oziel, L., Schourup-Kristensen, V., Wekerle, C. & Hauck, J. The pan-Arctic continental slope as an intensifying conveyer belt for nutrients in the central Arctic Ocean (1985–2015). *Glob. Biogeochem. Cycles* **36**, e2021GB007268 (2022).
97. Rogge, A. et al. Carbon dioxide sink in the Arctic Ocean from cross-shelf transport of dense Barents Sea water. *Nat. Geosci.* **16**, 82–88 (2023).
98. Seifert, M. et al. Interaction matters: bottom-up driver interdependencies alter the projected response of phytoplankton communities to climate change. *Glob. Change Biol.* **29**, 4234–4258 (2023).
99. Nissen, C., Timmermann, R., Hoppema, M., Gürses, Ö. & Hauck, J. Abruptly attenuated carbon sequestration with Weddell Sea dense waters by 2100. *Nat. Commun.* **13**, 3402 (2022).

100. Nissen, C. et al. Severe 21st-century ocean acidification in Antarctic Marine Protected Areas. *Nat. Commun.* **15**, 259 (2024).

101. Nissen, C., Timmermann, R., van Caspel, M. & Wekerle, C. Altered Weddell Sea warm- and dense-water pathways in response to 21st-century climate change. *Ocean Sci.* **20**, 85–101 (2024).

102. Tanioka, T. et al. Global patterns and predictors of C:N:P in marine ecosystems. *Commun. Earth Environ.* **3**, 271 (2022).

103. Wang, Q., Wekerle, C., Danilov, S., Wang, X. & Jung, T. A 4.5 km resolution Arctic Ocean simulation with the global multi-resolution model FESOM 1.4. *Geosci. Model Dev.* **11**, 1229–1255 (2018).

104. Meinshausen, M. et al. Historical greenhouse gas concentrations for climate modelling (CMIP6). *Geosci. Model Dev.* **10**, 2057–2116 (2017).

105. Hausfather, Z. & Peters, G. P. Emissions – the 'business as usual' story is misleading. *Nature* **577**, 618–620 (2020).

106. Cram, J. A. et al. The role of particle size, ballast, temperature, and oxygen in the sinking flux to the deep sea. *Glob. Biogeochem. Cycles* **32**, 858–876 (2018).

107. Holmes, R. M. et al. Seasonal and annual fluxes of nutrients and organic matter from large rivers to the Arctic Ocean and surrounding seas. *Estuaries Coasts* **35**, 369–382 (2012).

108. Wadham, J. L. et al. Sources, cycling and export of nitrogen on the Greenland Ice Sheet. *Biogeosciences* **13**, 6339–6352 (2016).

109. Hopwood, M. J. et al. Review article: how does glacier discharge affect marine biogeochemistry and primary production in the Arctic? *Cryosphere* **14**, 1347–1383 (2020).

110. Wild, B. et al. Organic matter composition and greenhouse gas production of thawing subsea permafrost in the Laptev Sea. *Nat. Commun.* **13**, 5057 (2022).

111. Wilkenskjeld, S., Miesner, F., Overduin, P. P., Puglini, M. & Brovkin, V. Strong increase in thawing of subsea permafrost in the 22nd century caused by anthropogenic climate change. *Cryosphere* **16**, 1057–1069 (2022).

112. Matsuoka, A. et al. Pan-Arctic optical characteristics of colored dissolved organic matter: tracing dissolved organic carbon in changing Arctic waters using satellite ocean color data. *Remote Sens. Environ.* **200**, 89–101 (2017).

113. Planchat, A. et al. The representation of alkalinity and the carbonate pump from CMIP5 to CMIP6 Earth system models and implications for the carbon cycle. *Biogeosciences* **20**, 1195–1257 (2023).

114. Séférian, R. et al. Evaluation of CNRM Earth System Model, CNRM-ESM2-1: role of earth system processes in present-day and future climate. *J. Adv. Model. Earth Syst.* **11**, 4182–4227 (2019).

115. Lewis, K. M. & Arrigo, K. R. Ocean color algorithms for estimating chlorophyll a, CDOM absorption, and particle backscattering in the Arctic Ocean. *J. Geophys. Res. Oceans* **125**, e2019JC015706 (2020).

116. Arrigo, K. R. & van Dijken, G. L. Secular trends in Arctic Ocean net primary production. *J. Geophys. Res. Oceans* **116** (2011).

117. Ardyna, M. & Arrigo, K. R. Phytoplankton dynamics in a changing Arctic Ocean. *Nat. Clim. Change* **10**, 892–903 (2020).

118. Ardyna, M. et al. Under-ice phytoplankton blooms: shedding light on the 'invisible' part of Arctic primary production. *Front. Mar. Sci.* **7**, 608032 (2020).

119. Ardyna, M. et al. Environmental drivers of under-ice phytoplankton bloom dynamics in the Arctic Ocean. *Elementa* **8**, 30 (2020).

120. Sánchez-García, L. et al. Characterisation of three regimes of collapsing Arctic ice complex deposits on the SE Laptev Sea coast using biomarkers and dual carbon isotopes. *Permafr. Periglac. Process.* **25**, 172–183 (2014).

121. Vonk, J. E. et al. High biolability of ancient permafrost carbon upon thaw. *Geophys. Res. Lett.* **40**, 2689–2693 (2013).

122. Sanders, T. et al. Seasonal nitrogen fluxes of the Lena River Delta. *Ambio* **51**, 423–438 (2022).

123. Sánchez-García, L. et al. Inventories and behavior of particulate organic carbon in the Laptev and East Siberian seas. *Glob. Biogeochem. Cycles* **25** (2011).

124. Brüchert, V. et al. Carbon mineralization in Laptev and East Siberian sea shelf and slope sediment. *Biogeosciences* **15**, 471–490 (2018).

125. Holmes, R. M. et al. Lability of DOC transported by Alaskan rivers to the Arctic Ocean. *Geophys. Res. Lett.* **35**, 3–7 (2008).

126. Dittmar, T., Fitznar, H. P. & Kattner, G. Origin and biogeochemical cycling of organic nitrogen in the eastern Arctic Ocean as evident from D- and L-amino acids. *Geochim. Cosmochim. Acta* **65**, 4103–4114 (2001).

127. Dittmar, T. Evidence for terrigenous dissolved organic nitrogen in the Arctic deep sea. *Limnol. Oceanogr.* **49**, 148–156 (2004).

128. Hansell, D. A., Kadko, D. & Bates, N. R. Degradation of terrigenous dissolved organic carbon in the western Arctic Ocean. *Science* **304**, 858–861 (2004).

129. Letscher, R. T., Hansell, D. A., Kadko, D. & Bates, N. R. Dissolved organic nitrogen dynamics in the Arctic Ocean. *Mar. Chem.* **148**, 1–9 (2013).

130. Alling, V. et al. Nonconservative behavior of dissolved organic carbon across the Laptev and East Siberian seas. *Glob. Biogeochem. Cycles* **24** (2010).

131. Azam, F., Smith, D. C., Steward, G. F. & Hagström, Å. Bacteria–organic matter coupling and its significance for oceanic carbon cycling. *Microb. Ecol.* **28**, 167–179 (1994).

132. Jiao, N. et al. Microbial production of recalcitrant dissolved organic matter: long-term carbon storage in the global ocean. *Nat. Rev. Microbiol.* **8**, 593–599 (2010).

133. Xenopoulos, M. A. et al. How humans alter dissolved organic matter composition in freshwater: relevance for the Earth's biogeochemistry. *Biogeochemistry* **154**, 323–348 (2021).

134. Helms, J. R. et al. Absorption spectral slopes and slope ratios as indicators of molecular weight, source, and photobleaching of chromophoric dissolved organic matter. *Limnol. Oceanogr.* **53**, 955–969 (2008).

135. Chupakova, A. A., Chupakov, A. V., Neverova, N. V., Shirokova, L. S. & Pokrovsky, O. S. Photodegradation of river dissolved organic matter and trace metals in the largest European Arctic estuary. *Sci. Total Environ.* **622–623**, 1343–1352 (2018).

136. Juhls, B. et al. Dissolved organic matter at the fluvial–marine transition in the Laptev Sea using in situ data and ocean colour remote sensing. *Biogeosciences* **16**, 2693–2713 (2019).

137. Stein, R. & MacDonald, R. W. in *The Organic Carbon Cycle in the Arctic Ocean* (eds Stein, R. & MacDonald, R. W.) 315–322 (Springer, 2004).

138. Mouw, C. B., Barnett, A., McKinley, G. A., Gloege, L. & Pilcher, D. Global ocean particulate organic carbon flux merged with satellite parameters. *Earth Syst. Sci. Data* **8**, 531–541 (2016).

139. Manizza, M., Menemenlis, D., Zhang, H. & Miller, C. E. Modeling the recent changes in the Arctic Ocean CO_2 sink (2006–2013). *Glob. Biogeochem. Cycles* **33**, 420–438 (2019).

140. MacGilchrist, G. A. et al. The Arctic Ocean carbon sink. *Deep-Sea Res. I* **86**, 39–55 (2014).

141. Oziel, L. Climate change and terrigenous inputs decrease the efficiency of the future Arctic Ocean's biological carbon pump (v1.0). *Zenodo* https://doi.org/10.5281/zenodo.14228166 (2024).

Acknowledgements

Author contributions

Funding

Competing interests

The authors declare no competing interests.

Additional information

Extended data is available for this paper at https://doi.org/10.1038/s41558-024-02233-6.

Supplementary information The online version contains supplementary material available at https://doi.org/10.1038/s41558-024-02233-6.

Correspondence and requests for materials should be addressed to Laurent Oziel.

Peer review information *Nature Climate Change* thanks Diane Lavoie, Moritz Mathis and the other, anonymous, reviewer(s) for their contribution to the peer review of this work.

Reprints and permissions information is available at www.nature.com/reprints.
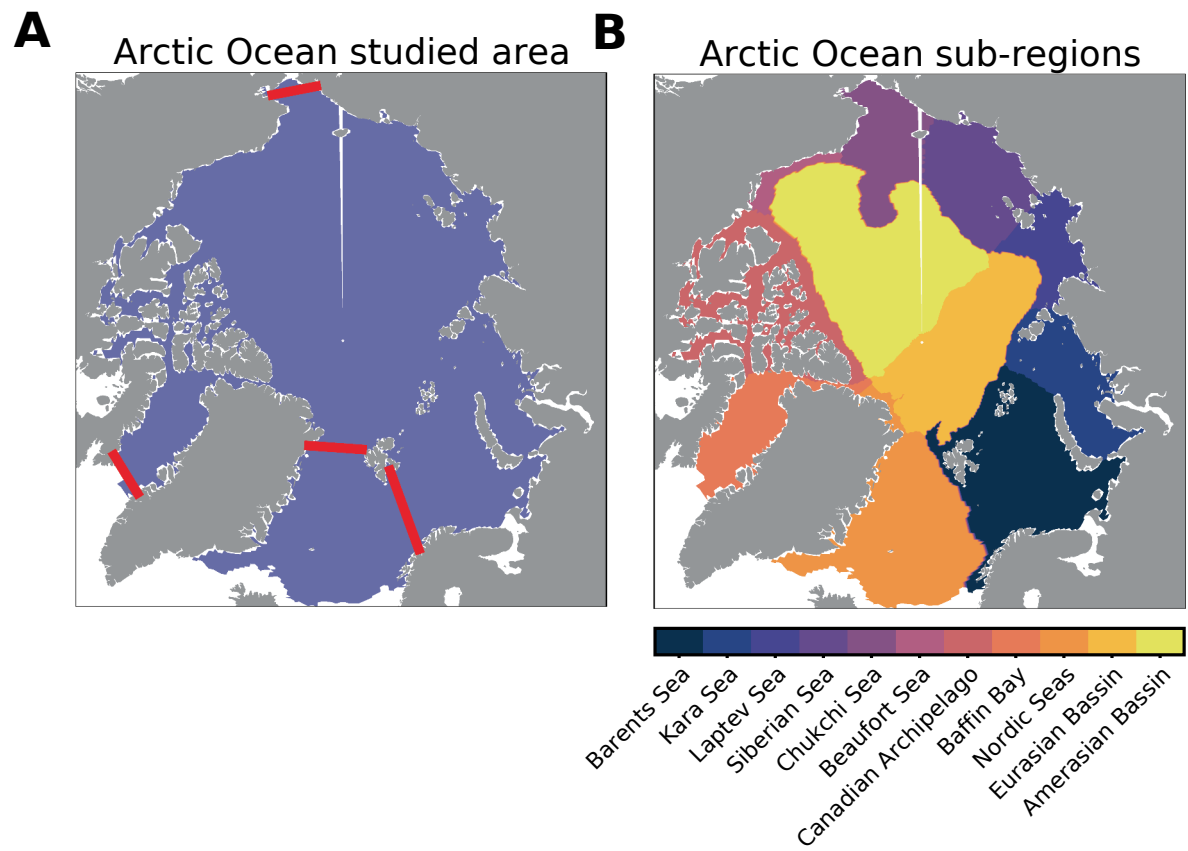
Extended Data Table 1 | Experimental design

Simulations	forcing	terrigenous inputs	coastal erosion pools	freshwater runoffs	year span
CTRL	looping over 1950-1959	constant	DIN, DIC	constant	1970-2100
EXP-1 (NoTerr)	historical + SSP3-7.0	none	DIN, DIC	constant	1970-2100
EXP-2	historical + SSP3-7.0	constant	DIN, DIC	constant	1970-2100
EXP-3 (Terr)	historical + SSP3-7.0	varying	DIN, DIC	varying	1970-2100
EXP-4	historical + SSP5-8.5	varying	DIN, DIC	varying	1970-2100
EXP-5	historical + SSP1-2.6	varying	DIN, DIC	varying	1970-2100
EXP-6	historical + SSP2-4.5	varying	DIN, DIC	varying	1970-2100
EXP-7	historical	varying	DON, DOC	varying	1970-2014
EXP-8	historical	varying	PON, POC	varying	1970-2014
EXP-9 (Cram et al. 2018)	historical	varying	DIN, DIC	varying	1970-2014
EXP-10 (no CDOM absorption)	historical	varying	DIN, DIC	varying	2010-2014

Full exhaustive experimental set-up with all simulations for sensitivity tests. The model was spun up for 50 years including four cycles of the 1950s decade, and one of the 1960s decade. The control run use constant atmospheric CO_2 concentration of 312.82 ppm (1950). Analysis started in 1970.

Extended Data Table 2 | Nitrogen and Carbon budgets

processes (Nitrogen:Carbon)	climate change	terrigenous inputs	scenario uncertainty	baseline (2090s, Terr)
Phytoplankton assimilation / NPP	9.3: 302	7.9: 124	4.7: 122	31.7: 706
Phytoplankton aggregation	2.1: 27	4.0: 35	2.7: 25	16.3: 120
Phytoplankton Excretion	9.2: 211	3.0: 60	4.15: 102	28.8: 520
Zooplankton Grazing	1.1: 24	1.9: 12	1.9: 15	9.4: 58
Zooplankton losses	1.26: 34	2.0: 12	1.9: 15	9.6: 62
Ocean Remineralization	13.2: 220	6.5: 64	4.5: 99	43.2: 623
Dissolution	1.4: 11	1.2: 5.3	0.52: 5	9.4: 60
Benthic Remineralization	6.6: 33	5.5: 24	3.6: 24	18.1: 101
Export flux 100m	−0.04: 4.1	0.5: 4.5	−0.4: −0.3	7.7: 53
Export flux 600m	−0.06: 0.45	0.05: 0.52	−0.09: −0.3	1.0: 7.3
Benthic dénitrification	0.06: NA	0.26: NA	0.13: NA	0.82: NA
CO$_2$ uptake	NA: 171	NA: −33	NA: 94	NA: 281

Quantification of the absolute contribution of climate change, terrigenous inputs and scenario uncertainty on some biogeochemical processes expressed both in terms of nitrogen [Tg N yr^{-1}] and carbon [TgC yr^{-1}]. Phytoplankton losses encompass excretion and aggregation. Zooplankton losses encompass mortality, excretion, sloppy feeding, and faecal loss.

A Arctic Ocean studied area **B** Arctic Ocean sub-regions

Barents Sea · Kara Sea · Laptev Sea · Siberian Sea · Chukchi Sea · Beaufort Sea · Canadian Archipelago · Baffin Bay · Nordic Seas · Eurasian Bassin · Amerasian Bassin
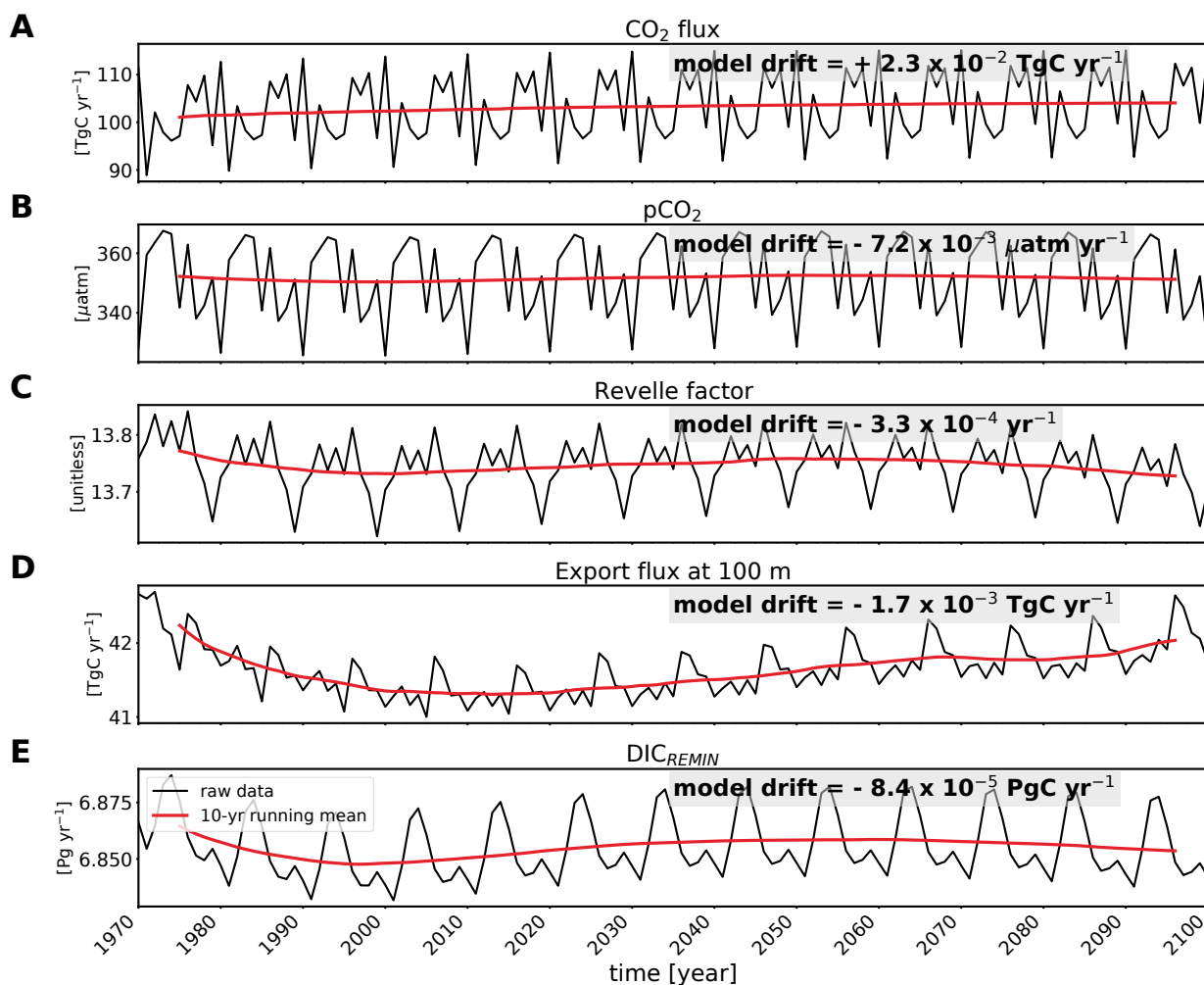
Extended Data Fig. 1 | Studied area. The studied area of the Arctic Ocean represented in **A** by the colored area. The studied area is subdivided in **B** 11 regions. The regionalization is not used in the main manuscript but serves in the assessment of the modeled versus satellite-derived NPP. Red lines are transects representing the boundary of the Arctic region used for volume and nutrient transport (Supplementary Table 3) in order to be consistent with observations.
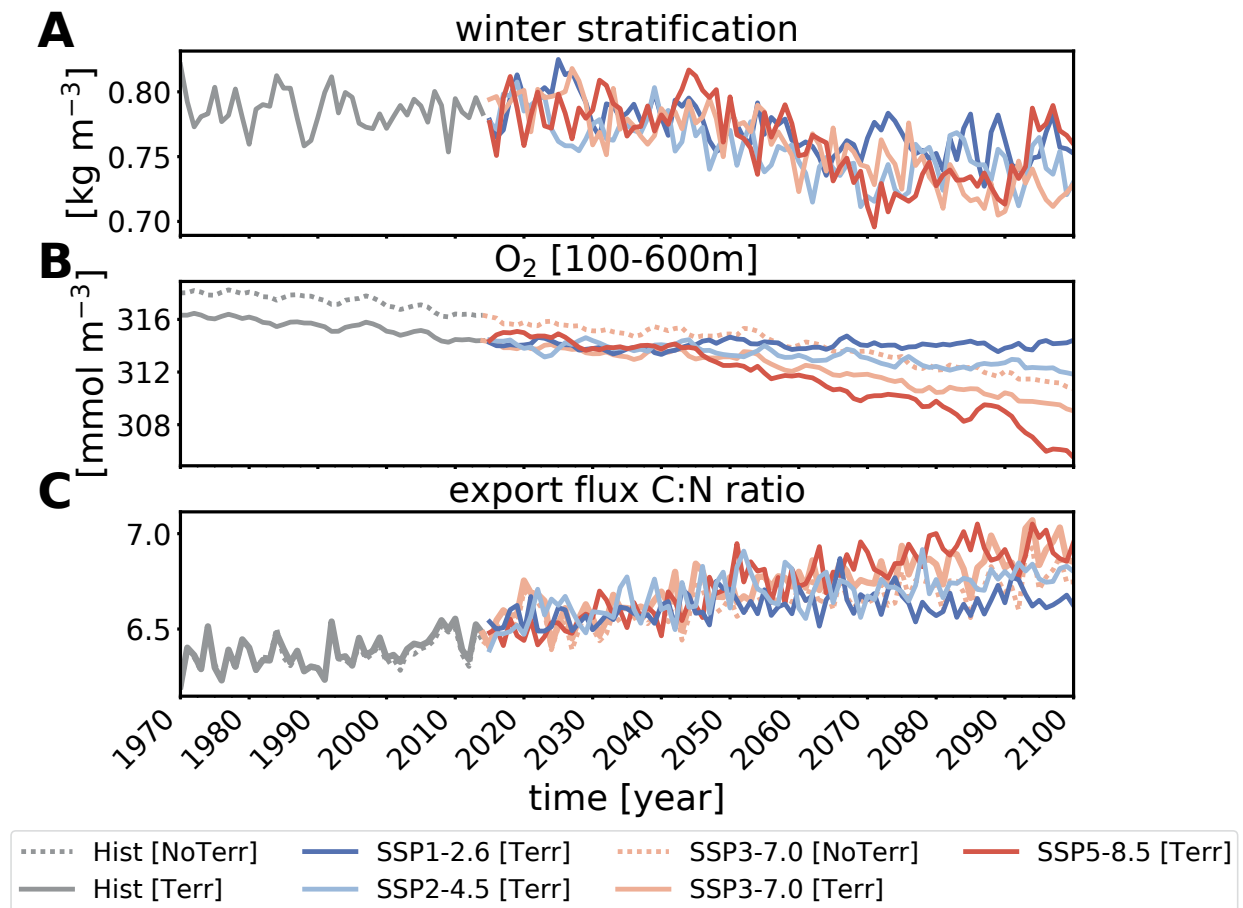
Extended Data Fig. 2 | Characteristics of the 'New' Arctic Ocean. Time-series of **A** stratification (potential density difference between 300 m and surface) in winter [kg m^{-3}], **B** upper mesopelagic (100-600 m) oxygen concentration [mmol m^{-3}] and **C** the stoichiometric carbon to nitrogen (C:N) ratio of the export flux at 100 m. Our model simulations allow flexible stoichiometry. The observed increasing C:N ratios, in line with a nutrient poorer environment, is limiting the decrease of the BCP efficiency. In fixed stoichiometry model, the dampening of the BCP would therefore be over-estimated.
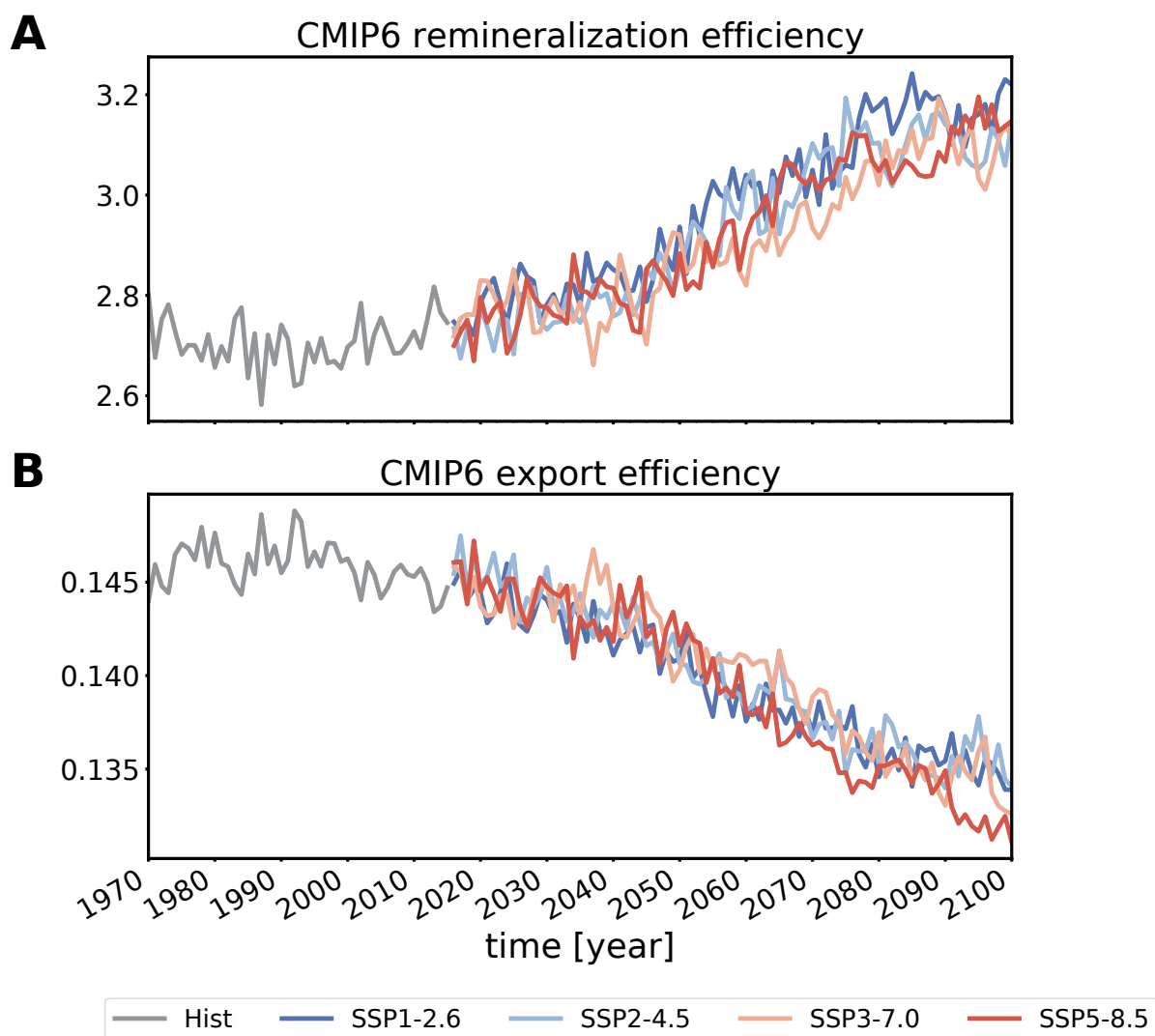
A
CO$_2$ flux

model drift = + 2.3 x 10^{-2} TgC yr^{-1}

B
pCO$_2$

model drift = - 7.2 x 10^{-3} μatm yr^{-1}

C
Revelle factor

model drift = - 3.3 x 10^{-4} yr^{-1}

D
Export flux at 100 m

model drift = - 1.7 x 10^{-3} TgC yr^{-1}

E
DIC$_{REMIN}$

model drift = - 8.4 x 10^{-5} PgC yr^{-1}

raw data
10-yr running mean

time [year]

Extended Data Fig. 3 | Estimation of the model drift. Timeseries from our control simulation (constant climate and atmospheric CO$_2$ concentration) for **A** ocean CO$_2$ uptake [TgC yr^{-1}], **B** partial pressure of CO$_2$ in the surface ocean [µatm yr^{-1}], **C** Revelle factor [yr^{-1}], **D** export flux at 100 m [TgC yr^{-1}], and **C** DIC$_{REMIN}$ [PgC yr^{-1}]. The model drift is extremely small compare to climate change and evidence a quasi-equilibrium for surface (CO$_2$ flux, p_{CO_2} and Revelle factor), intermediate (export flux at 100 m) and deep ocean variables (DIC$_{REMIN}$).
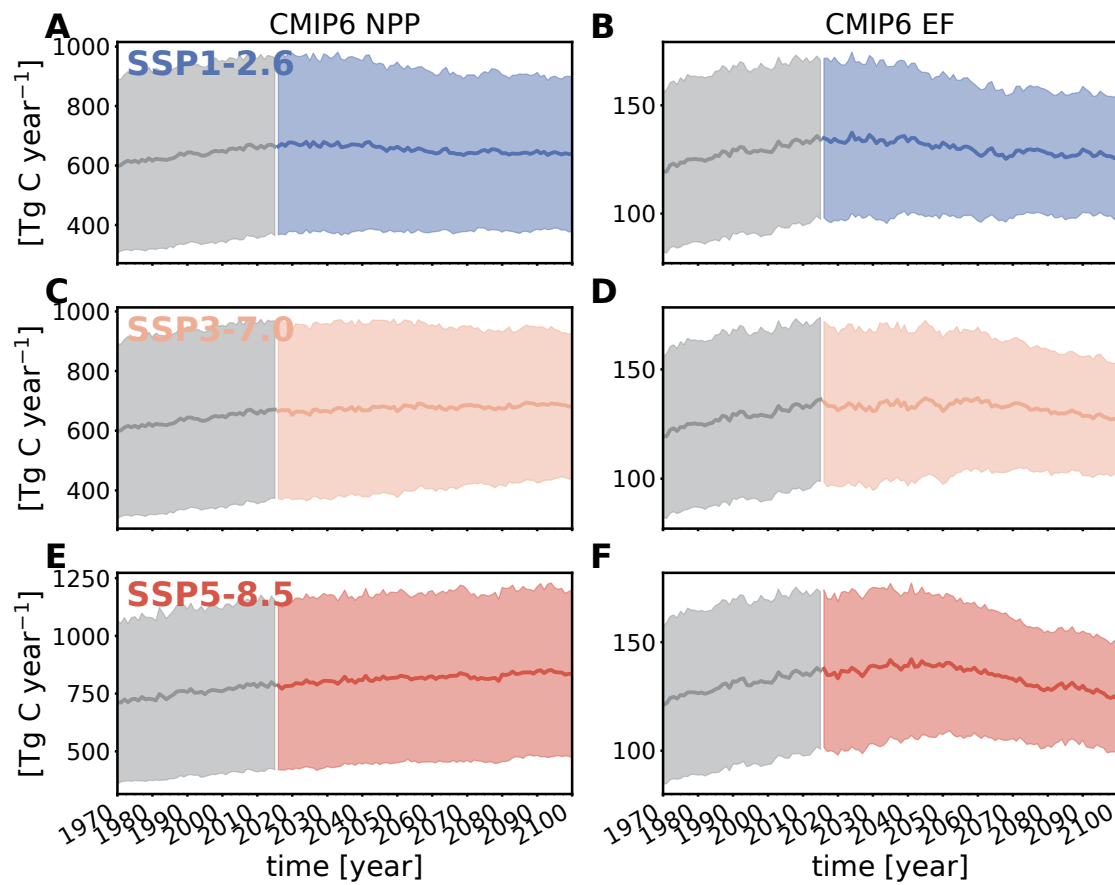
Extended Data Fig. 4 | CMIP6 assessment of NPP and export flux. Timeseries of the CMIP6 ensemble mean (and ± 1 standard deviation) of Net primary Production (NPP) and export flux (EF) for the historical period plus 3 emission scenarios (**A, B**) SSP1-2.6; (**C, D**) SSP3-7.0; (**E, F**) SSP5-8.5. Historical periods and SSP1-2.6 and SSP3-7.0 (**A, B, C, D**) used 16 models [ACCESS-ESM1-5; CanESM5-1; CanESM5-CanOE; CanESM5; CESM2; CESM2-WACCM; CNRM-ESM2-1; GFDL-ESM4; IPSL-CM5A2-INCA; IPSL-CM6A-LR; MIROC-ES2L; MPI-ESM1-2-HR; MPI-ESM1-2-LR; NorESM2-LM; NorESM2-MM; UKESM1-0-LL] while the SSP5-8.5 (**E, F**) has 17, the additional model being [MRI-ESM2-0].

A CMIP6 remineralization efficiency

B CMIP6 export efficiency

Hist — SSP1-2.6 — SSP2-4.5 — SSP3-7.0 — SSP5-8.5

Extended Data Fig. 5 | CMIP6 assessment of remineralization and export efficiencies. Time series of the (carbon-based) **A** remineralization and **B** export efficiencies from the CMIP6 (Coupled Model Intercomparison Project) ensemble. Only 5 models from 3 different Earth System model providers delivered remineralization as an output. For consistency, we limited the analysis to those 5 models: CESM2, CESM2-WACCM, IPSL-CM6A-LR, MPI-ESM1-2-HR, MPI-ESM1-2-LR. The analysis shows that our results are consistent with those of CMIP6 models.
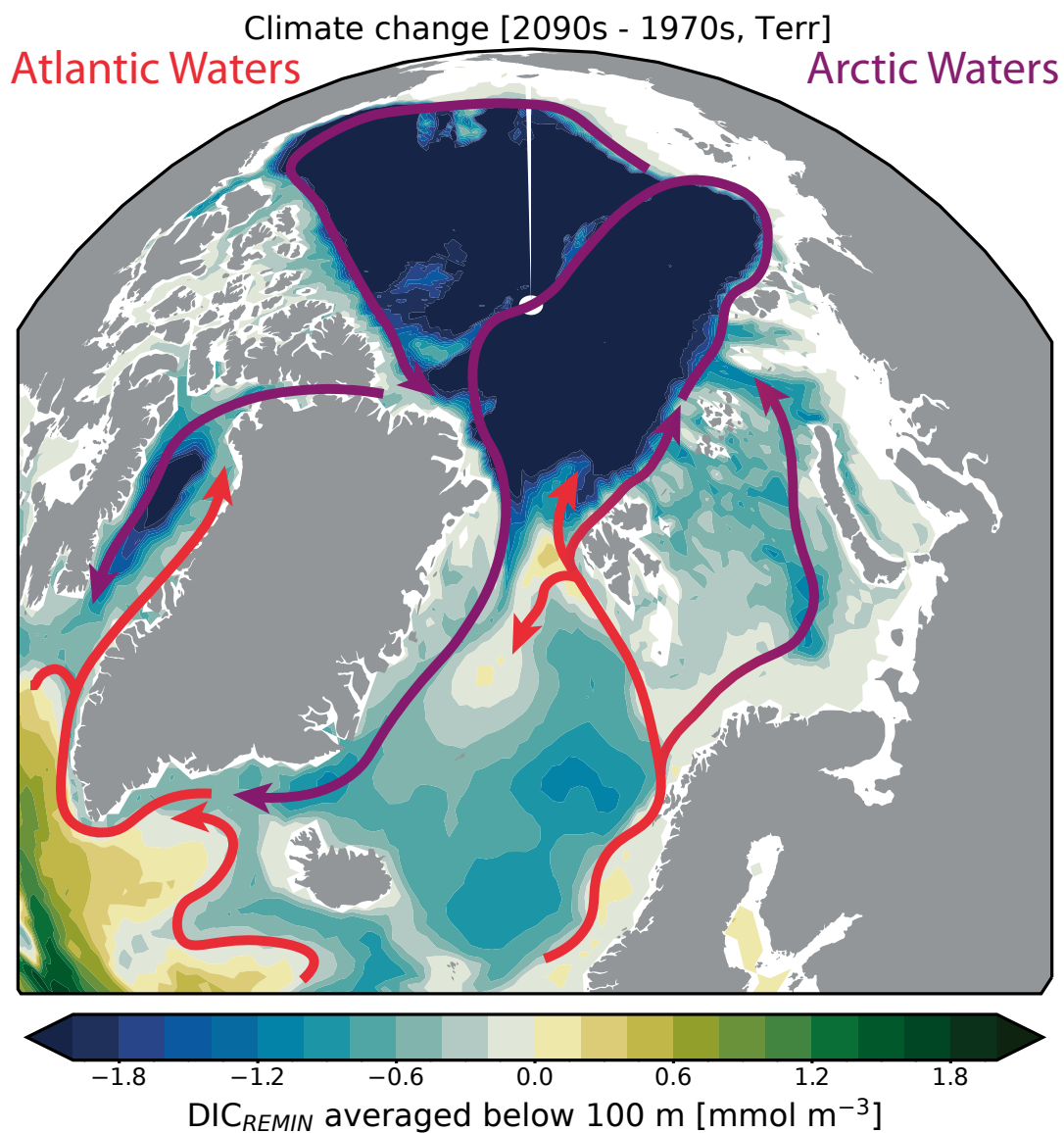
Extended Data Fig. 6 | Temporal change (climate change) in the spatial distribution of the average DIC$_{REMIN}$ below 100 m. This map shows a dipole structure between the Arctic Ocean and the North Atlantic Ocean. The Arctic Ocean is losing DIC$_{REMIN}$ while the North Atlantic is gaining DIC$_{REMIN}$. The European Arctic Corridor is the major gateway where 80% of all water masses which enter or leave the Arctic Ocean take place. This analysis demonstrates that the negative DIC$_{REMIN}$ anomaly in the Arctic Ocean is produced locally and not imported from adjacent Seas. By contrast, the Arctic Ocean is exporting southward negative DIC$_{REMIN}$ anomalies to the North Atlantic.
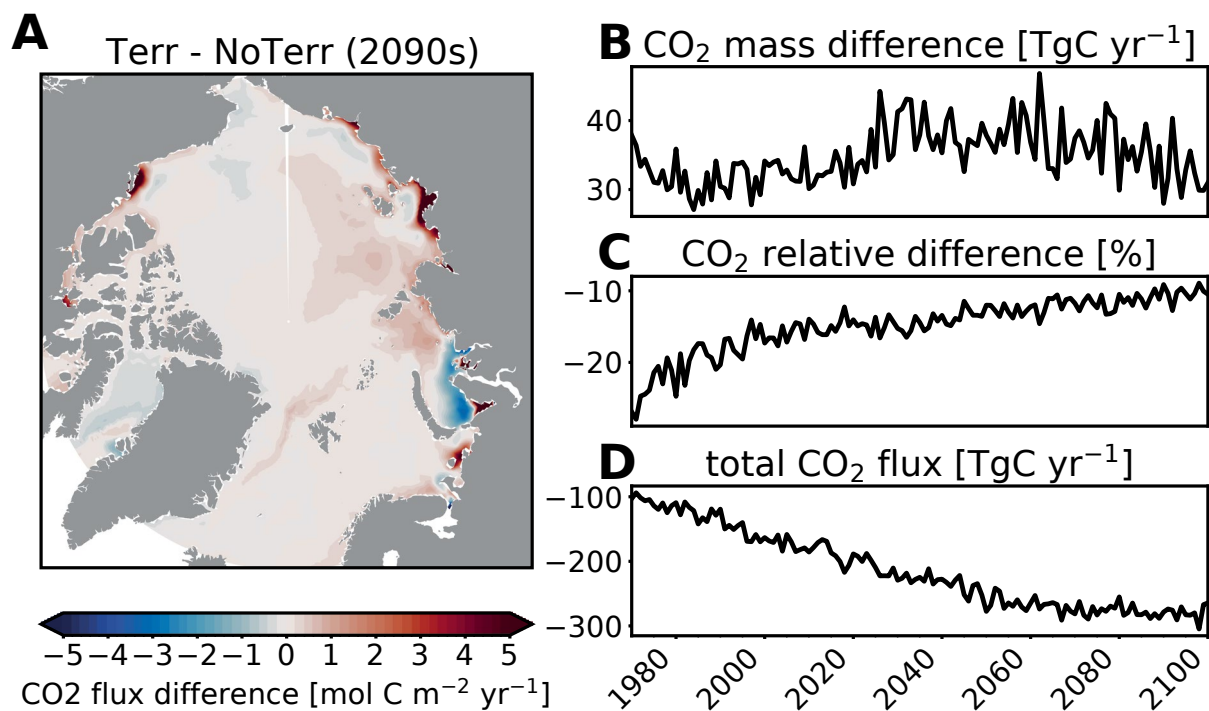
Extended Data Fig. 7 | Spatio-temporal changes in air-sea CO_2 fluxes due to terrigenous inputs. A Map showing the contribution of terrigenous inputs on air-sea CO_2 fluxes [molC m^{-2} yr^{-1}]. Positive anomalies (red colors) indicate regions where *Terr* is showing more outgassing (or less uptake) than *NoTerr*. The associated time series on the right-hand side show the **B** absolute [TgC yr^{-1}], **C** relative [%] differences between *Terr* and *NoTerr* and **D** the total AO carbon

sink of the baseline *Terr* simulation (a negative flux means uptake by the ocean). The total amount of CO_2 released to the atmosphere due to terrigenous inputs fluctuated around 27-47 TgC yr^{-1} in the *Terr* simulation. Given the AO carbon sink increases with climate change, the relative reduction of the AO carbon sink due to terrigenous inputs decreased from about 23.2% in the 1970s to about 10.3% in the 2090s.